Energy, Mines and Resources Canada
Canada Centre for Remote Sensing

Énergie, Mines et Ressources Canada
Centre Canadien de Télédétection

HEAT CAPACITY MAPPING MISSION (HCMM): INTERPRETATION OF IMAGERY OVER CANADA

Josef Cihlar, Principal Investigator
R. Grant Dixon, Co-Author

Energy, Mines and Resources Canada,
Canada Centre for Remote Sensing,
717 Belfast Road,
Ottawa, Ontario.
K1A 0Y7

August 1981

Type III Final Report

Prepared for:

NASA,
Goddard Space Flight Center,
Greenbelt, Maryland, 20771, U.S.A.

TECHNICAL REPORT STANDARD TITLE PAGE

1. Report No.	2. Government Accession No.	3. Recipient's Catalog No.

4. Title and Subtitle	5. Report Date
HEAT CAPACITY MAPPING MISSION (HCMM): INTERPRETATION OF IMAGERY OVER CANADA	AUGUST 1981
	6. Performing Organization Code

7. Author(s)	8. Performing Organization Report No.
J. CIHLAR AND R.G. DIXON	

9. Performing Organization Name and Address	10. Work Unit No.
ENERGY, MINES AND RESOURCES CANADA, CANADA CENTRE FOR REMOTE SENSING, 2464 SHEFFIELD ROAD, OTTAWA, ONTARIO. K1A 0Y7	11. Contract or Grant No.
	13. Type of Report and Period Covered
12. Sponsoring Agency Name and Address ENERGY, MINES AND RESOURCES CANADA	TYPE III FINAL REPORT
	14. Sponsoring Agency Code

15. Supplementary Notes

16. Abstract

The purpose of this study was to assess the potential of the Heat Capcity Mapping Mission (HCMM) satellite thermal infrared data for monitoring soil water status over large areas, and to evaluate the influence of other surface and environmental parameters on the satellite images. HCMM images were acquired over two sites in Canada. Supporting aircraft and ground data were obtained at a smaller subsite in Alberta. Visual analysis of a large number of images showed that nighttime surface temperature distribution was primarily related to the near-surface air temperature; the effects of topography, wind, and land cover were low or indirect through air temperature. Surface cover and large altitudinal differences were important parameters influencing daytime apparent temperature values. A quantitative analysis of the relationship between the Antecedent Precipitation Index and the satellite thermal IR measurements did not yield statistically significant correlation coefficients, but the correlations had a definite temporal trend which could be related to the increasing uniformity of vegetation cover. The large pixel size (resulting in a mixture of cover types and soil/canopy temperatures measured by the satellite) and high cloud cover frequency found in images covering both Canadian sites and northern U.S. were considered the main deficiencies of the thermal satel-

17. Key Words (Selected by Author(s))	18. Distribution Statement
HCMM, cover type, soil moisture, surface temperature, cloud cover, topographic effects	

19. Security Classif. (of this report)	20. Security Classif. (of this page)	21. No. of Pages	22. Price*
UNCLASSIFIED	UNCLASSIFIED	62	

*For sale by the Clearinghouse for Federal Scientific and Technical Information, Springfield, Virginia 22151.

Enclosure

TECHNICAL REPORT STANDARD TITLE PAGE

Continuation

16. Abstract

lite data. Since the frequent clouds render a significant proportion of data unsuitable for a quantitative analysis, it is concluded that satellite thermal IR data could not be the primary remote sensing data source in an operational soil moisture monitoring system for the areas studied. However, high resolution thermal IR data might supplement other sources of information provided that suitable preprocessing and analysis algorithms can be developed.

HEAT CAPACITY MAPPING MISSION (HCMM): INTERPRETATION OF IMAGERY OVER CANADA

Josef Cihlar, Principal Investigator
R. Grant Dixon, Co-Author

Energy, Mines and Resources Canada,
Canada Centre for Remote Sensing,
717 Belfast Road,
Ottawa, Ontario.
K1A 0Y7

August 1981

Type III Final Report

Prepared for:

NASA,
Goddard Space Flight Center,
Greenbelt, Maryland, 20771, U.S.A.

TABLE OF CONTENTS

ABSTRACT

The purpose of this study was to assess the potential of the Heat Capacity Mapping Mission (HCMM) satellite thermal infrared data for monitoring soil water status over large areas, and to evaluate the influence of other surface and environmental parameters on the satellite images. HCMM images were acquired over two sites in Canada. Supporting aircraft and ground data were obtained at a smaller subsite in Alberta. Visual analysis of a large number of images showed that nighttime surface temperature distribution was primarily related to the near-surface air temperature; the effects of topography, wind, and land cover were low or indirect through air temperature. Surface cover and large altitudinal differences were important parameters influencing daytime apparent temperature values. A quantitative analysis of the relationship between the Antecedent Precipitation Index and the satellite thermal IR measurements did not yield statistically significant correlation coefficients, but the correlations had a definite temporal trend which could be related to the increasing uniformity of vegetation cover. The large pixel size (resulting in a mixture of cover types and soil/canopy temperatures measured by the satellite) and high cloud cover frequency found in images covering both Canadian sites and northern U.S. were considered the main deficiencies of the thermal satellite data. Since the frequent clouds render a significant proportion of data unsuitable for a quantitative analysis, it is concluded that satellite thermal IR data could not be the primary remote sensing data source in an operational soil moisture monitoring system for the areas studied. However, high resolution thermal IR data might supplement other sources of information provided that suitable preprocessing and analysis algorithms can be developed.

ACKNOWLEDGEMENTS

Numerous individuals contributed to this study. Cal Bricker was instrumental in organizing and funding the supporting aircraft study. Colin MacKenzie, Neil Clark and their staff provided much of the ground data collected over the Alberta site. Locke Stuart and Richard Stonesifer assisted in providing HCMM data from GSFC and in resolving problems we have encoutered.

Julie Harvie, Harvey Thorleifsson, Diane Robert, Sandy Hay, and Tim Lynham participated in HCMM data reduction and analysis. Bert Guindon assisted with digital registration procedures. Excellent typing support was provided by Marion Armitage.

We thank all these persons for their assistance.

LIST OF TABLES

LIST OF FIGURES

1. INTRODUCTION

The amount of water present in the soil is of interest to most human activities involving the land. A number of different uses for soil moisture information exist in agriculture, hydrology, and climatology (Cihlar, 1978).

Due to large spatial and temporal variability of soil moisture, the traditional point measurements do not give representative estimates over extended areas. In this respect, remote sensing techniques have an inherent advantage because they permit viewing the entire area of interest and thus reducing the need for extrapolation.

Various remote sensing methods have been considered for soil moisture estimation. Since the known remote sensing techniques are directly sensitive only to near-surface water content (Cihlar, 1978, 1979) and since for many purposes one wishes to know the amount of water in the soil profile it has been suggested (e.g., Jackson et al, 1977) that plants could be used as indicators of soil water deficit. Given that a major effect of soil water deficit on sunlit transpiring plants is an increase in their temperature, remote sensing in the thermal infrared region is preferable over measurements in other spectral bands. In the absence of plants (i.e., bare soil), surface temperature of a wet soil is reduced (compared to a dry soil) during the day as a result of increased latent heat loss and/or increased thermal inertia (Cihlar et al, 1979). The net impact of increased water content in both cases (bare or vegetated soil) is a reduction of the maximum daytime surface temperature measured by a thermal scanner. It is important to note, however, that the two surface temperature vs. soil water relationships differ in the soil water (layers) considered as well as in the statistical parameters which describe these relationships.

To assess the potential of satellite thermal infrared data for monitoring soil water status over large areas and based on positive results of numerous previous studies (Jackson et al, 1978), a proposal has been submitted to the Heat Capacity Mapping Mission (HCMM) Program. The primary objective of the proposed study was to determine whether soil moisture distribution in a Northern Prairie agricultural area can be determined on the basis of the thermal inertia concept by using HCMM satellite data. Secondary objectives were assessments of the effects of topography, heterogenous surface cover, and season on soil moisture estimation. The proposal was accepted as Experiment HCM - 054 and an agreement was concluded between NASA and the Department of Energy, Mines and Resources Canada. The purpose of this report is to summarize work done under this project and to describe the results. Progress during the project has been reported previously (Cihlar, 1979; 1980a; 1980b).

2. METHODOLOGY

2.1 Satellite Data Acquisition

The HCMM satellite was placed into a sun-synchronous orbit on 26 April, 1978. In southern Canada, the overpass occurred shortly after 2:30 a.m. and 1:30 p.m. Local Solar Time. The Heat Capacity Mapping Radiometer (HCMR) recorded incident radiation in the reflectance (0.5 to 1.1 micrometers) and thermal infrared (10.5 to 12.5 micrometers) bands at spatial resolutions of about 500 and 600 m (square pixels), respectively. While both channels were recorded during the daytime overpass, only the thermal band was recorded at night.

The study area was located in southern Alberta and adjacent regions by latitudes 49°N and 54°N, and by longitudes 107°W and 121°W. In this area, the orbit configuration chosen for HCMM provided, every 15 days, about four day/night (12-hours apart) overpasses and about 10 day overpasses; the exact number of day/night coverages varied with latitude. The study area chosen contained a range of surface cover types, topographic and physiographic characteristics, as well as soil moisture conditions in dryland and irrigated areas.

A secondary study area was located in Quebec and Ontario. The area was irregular in shape and included St. Lawrence Lowlands and a part of Canadian Shield, and was approximately delineated by 44° to 48°N latitude and by 70° to 79°W longitude. This area is covered primarily by cultivated and built-up land in the south and is forested in the north. The data request specified that all acquired HCMM images be delivered as positive transparencies (maximum acceptable cloud cover was 100%).

Figures 1 through 4 show the number of scenes covering 1° x 1° cells which were delivered for the western and eastern sites, separately for day and night overpasses. Since many scenes with image centres outside the study area partly covered the area of interest, they were also delivered to the project. In preparing Figures 1 to 4, images have been catalogued according to the geographic coordinates of the image centre using a 1° latitude X 1° longitude grid, and the exact cells included in the image were then identified. For daytime scenes, all cases with one or both bands received were counted. Only three summer months (June, July, August) are shown because this period is of primary interest for soil moisture estimation from the agricultural viewpoint. About one-third of all images delivered were acquired during these three months.

Based on a preliminary analysis of the day and night images received, several sets were selected for digital analysis. These sets were each obtained within 12 hours, over the area of interest, during the summer period, and were reasonably cloud-free. Table 1 lists the sets ordered in digital form (including day-night temperature difference and apparent thermal inertia). Of these, only two western site sets and one eastern site scene were delivered (Table 1).

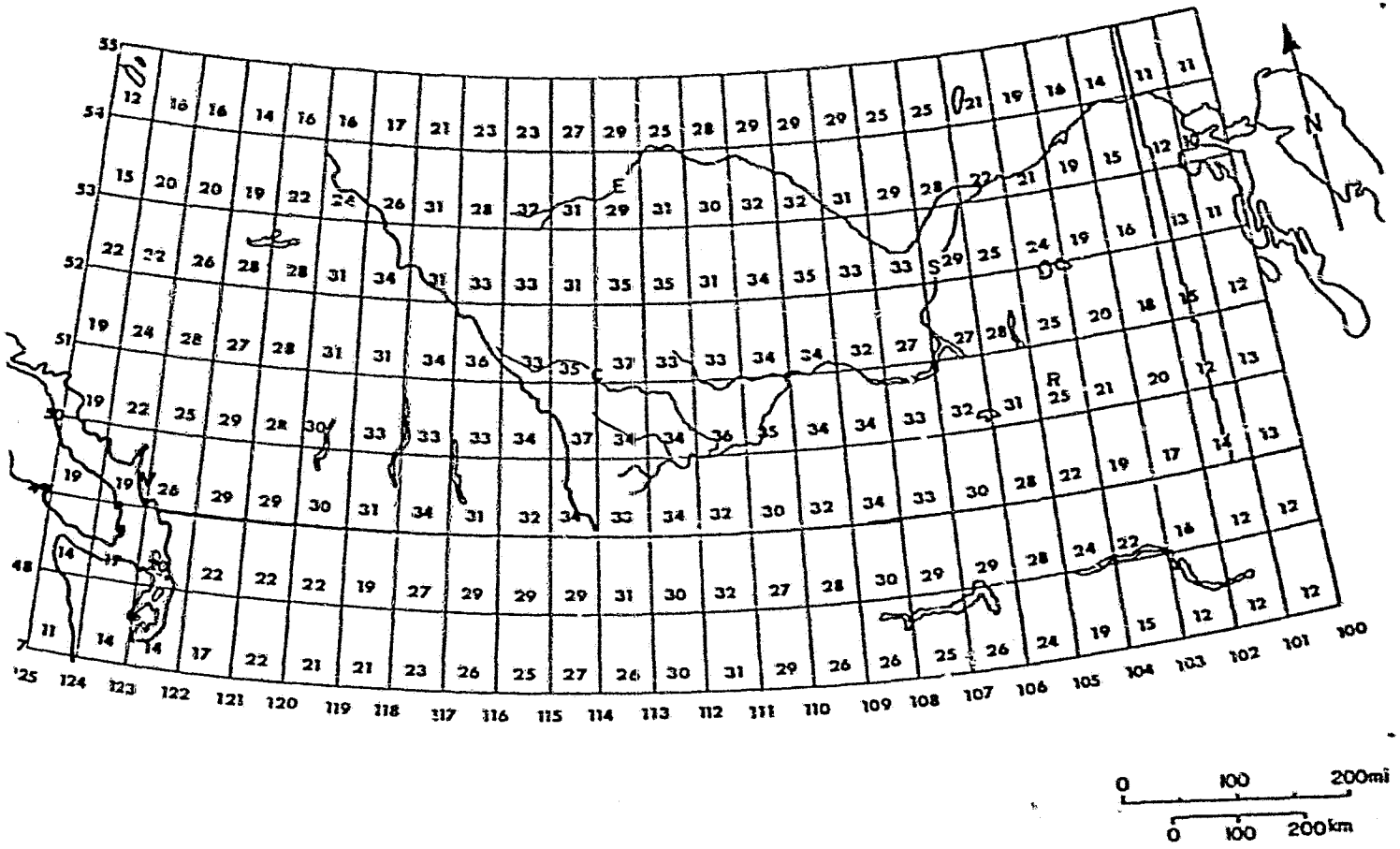

Figure 1: The total number of daytime scenes acquired during June, July and August 1978 over the western site.

E – Edmonton
C – Calgary
S – Saskatoon
R – Regina
V – Vancouver

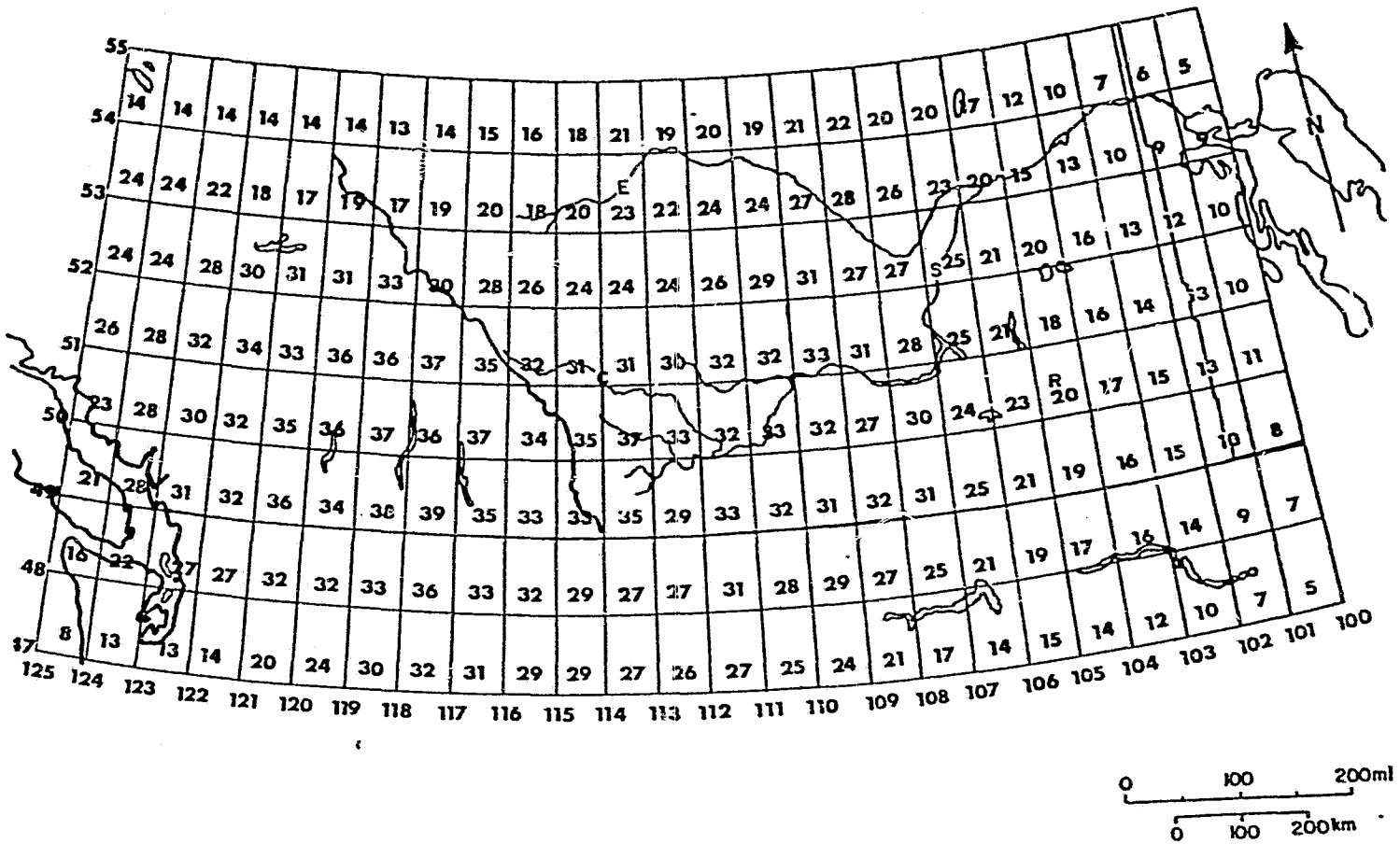

Figure 2: The total number of nightime scenes acquired during June, July and August 1978 over the western site.

E – Edmonton
C – Calgary
S – Saskatoon
R – Regina
V – Vancouver

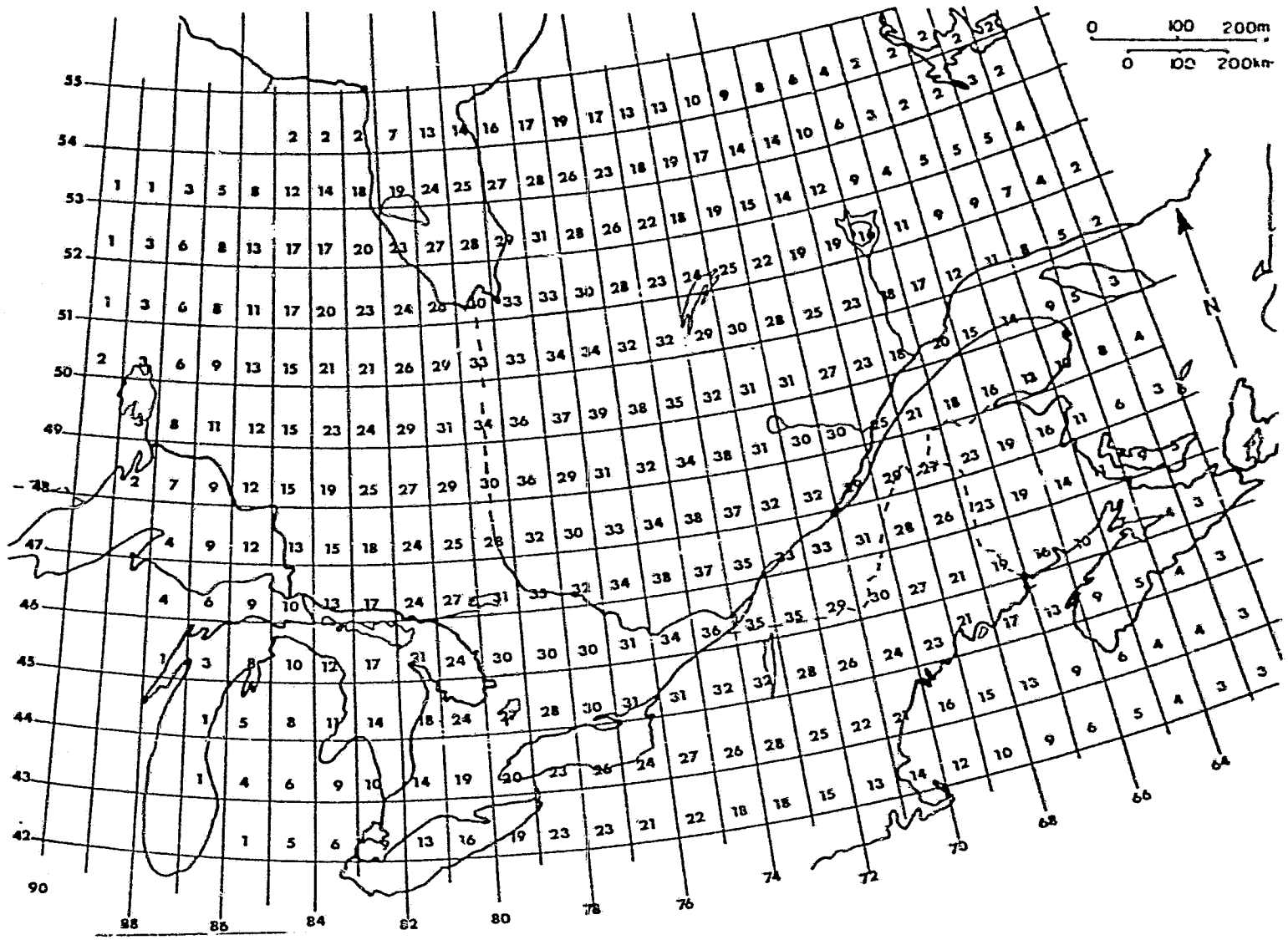

Figure 3: The total number of daytime scenes acquired during June, July and August 1978 over the eastern site.

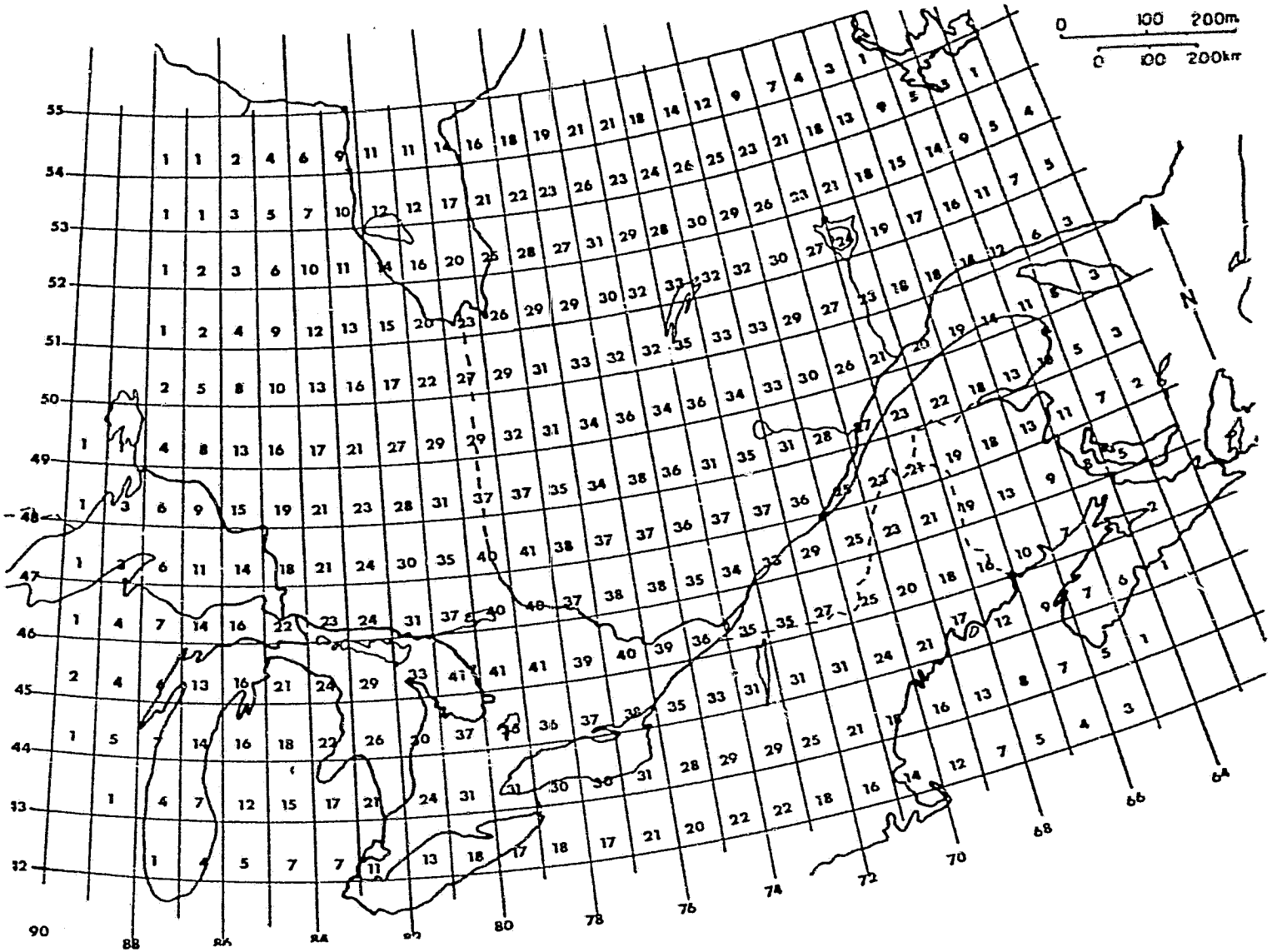

Figure 4: The total number of nightime scenes acquired during June, July and August 1978 over the eastern site.

TABLE 1

Requested and Received HCMM Digital Data

Date	Coordinates	Identification	Requested	Received
		Western Site		
14/06/78	N52-35/W116-20	AA0049-20580 1&2	X	X
14/06/78	N46-32/W113-59	AA0049-20570 1&2	X	X
	N52-10/W111-34	AA0049-09580-3	X	X
15/07/78	N48-10/W110-00	AA0080-20350 1&2	X	X
16/07/78	N53-32/W111-01	AA0081-09530-3	X	X
	N47-30/W113-26	AA0081-09550-3	X	X
		Eastern Site		
06/06/78	N44-47/W076-49	AA0041-18310 1&2	X	X
	N47-13/W076-54	AA0041-07340-3	X	X
06/06/78	N40-37/W071-01	AA0041-07310-6&7	NO	X
	N40-45/W071-01	AA0041-07310-8,4,5	NO	X
19/09/78	N47-01/W076-00	AA0146-17470-1&2	X	NO
	N45-29/W074-20	AA0147-07080-3	X	NO

A microfiche search of Landsat images acquired at the Prince Albert (Saskatchewan) Satellite Station was conducted to determine if clear-sky Landsat data coincident with HCMM overpasses were recorded. A good quality Landsat image was recorded on 22 June, 1978 over a portion of the western site which included irrigated agriculture and rangeland. This image was obtained in digital form and was subsequently used in the digital analysis of the HCMM data.

2.2 Supporting Data

In 1978 and 1979, a joint project was undertaken with the Irrigation Division of Alberta Agriculture and with the support of the Alberta Center for Remote Sensing which was aimed at determining the feasibility of plant moisture stress determination through airborne remote sensing. Airborne data collected during this study could also be used in the HCMM project. Table 2 gives an overview of airborne and ground data collected during this joint project. Soil samples for water content determination were collected, using a soil probe, at 30.5cm increments to a depth of 120 cm (150 cm for alfalfa during one mission). Sampling point locations (usually six per field and 12 for irrigated experimental plots) were marked on aerial photographs. Air temperature values were obtained on site or from nearby meteorological stations.

2.3 Data Processing

Upon reception, HCMM images were catalogued according to location and date (Figures 1 through 4). The images arrived over a period of time and in a random manner, and a systematic analysis could therefore not be undertaken until most images were delivered. Since many images were delivered in the early months of 1980, an inventory of the western site candidate scenes for visual and digital analysis was undertaken in April, 1980 (Cihlar, 1980a).

To perform visual analysis, suitable western study area scenes were arranged in a time sequence and analyzed in terms of the correspondence of image tones and patterns to known surface, physiographic and meteorological features. The objective of this analysis was to determine the important environmental parameters in the study area which influenced the radiation recorded by the HCMR. A limited semi-quantitative analysis of the images was also performed by using spot densitometer and the calibrating step-wedge provided on each transparency.

Digital HCMM data were first read into the CCRS Image Analysis System (CIAS; Goodenough, 1979) using the universal input format. A 1024 lines x 1024 pixel area was then selected on each image/date and stored on a unidisk file (algorithm TAPDSK). Data from 14/6/78 were initially registered (REGU) to the original 15/7/78 image by identifying ground control points visually on the image display. A sin(x)/x resampling algorithm was then selected (INTFUN) and used (OVRLYU) to produce a 14/6/78 image registered to the 15/7/78 original image.

TABLE 2

Alberta Centre for Remote Sensing/Alberta Agriculture/ Canada Centre for Remote Sensing Project

DATE	AIRBORNE		HCMM		LANDSAT	PRT-5
	CIR	TIR	IMAGES	DIGITAL		
14 June 1978				X		
21 June 1978	X	X				
22 June 1978		X			X	
15 July 1978				X		
5 August 1978	X	X				
6 August 1978		X				
Various 1978			X			X
18 July 1979	X	X				
18 July 1979		X				
6 August 1979	X	X				X
Various 1979						X

To register the 15/7/78 image to 1:250,000 topographic maps (UTM projection), ground control points (GCP's) were selected on these maps throughout the area and located on one of the HCMM bands (usually day reflectance and/or day thermal infrared). In this manner, a file of about 50 GCP's was built (GNDDAT). A nearest neighbour (NN) resampling algorithm was then selected (INTFUN) and all bands of the HCMM image were resampled (UTMREG) to produce a UTM-registered image with pixels 481.5m x 481.5m (cell size of the digital data provided by NASA). This image was then resampled using cubic convolution (CC) interpolation (RESROT) to produce pixels 350m x 350m. The smaller pixel size was produced to assess whether surface cover ambiguities could be reduced in this manner. The same GCP file was applied to both 15/7/78 and 14/6/78 images.

HCMM data for the eastern site (6/6/78) were handled in the same way as data for 15/7/78.

Landsat data for the western site (22/6/78) were first resampled (RESROT) using a nearest neighbour algorithm to produce pixels 175m x 175m. A GCP file was then generated (GNDDAT) with the aid of 1:250,000 topographic maps. A nearest neighbour resampling algorithm was selected (INTFUN) and applied (UTMREG) to register the 14/6/78 HCMM data and the 22/6/78 Landsat image.

The Anticedent Precipitation Index (API) was selected as the ground parameter describing soil water status. Based on readily available meteorological data, the API for a given day was calculated as:

$$API = \sum_{i=0}^{n} k^i P_i ,$$

where P - precipitation in millimetres and n - 30 is the number of days prior to the date of interest for which moisture depletion was calculated. In computer form, API for day i was calculated as:

$$API\ (i) = API\ (i - 1)k + P(i).$$

Values of k between 0.75 and 0.95 (at 0.05 intervals) were used in the computations (Section 3). These calculations were performed for 42 meteorological stations in the western study area for which daily precipitation values were available, for both 14 June and 15 July 1978 target dates. The same calculation was carried out for 65 meteorological stations at the eastern site and the target date of 6 June, 1978.

Aircraft thermal scanner data were digitized and recorded on CCTs, including calibration signals from two internal reference plates. After the digital data were displayed on the CIAS, digital values were extracted over the sites sampled on the ground and were converted to apparent temperatures using values from the reference

plates. This procedure was applied separately for day and night overflights where possible, and the day minus night temperature difference was then calculated. Since in several cases no nighttime scanner data were available (due to weather, instrument malfunction or problems in digitization), the daytime apparent surface minus maximum air temperature difference ΔT_{da} was computed for all data and subsequently used in the analysis. The procedures for aircraft data analysis were described in detail by Cihlar et al. (1979).

For the analysis of airborne data, soil water content was quantified as Plant Available Water (PAW) expressed as the fraction of the maximum possible plant-available water for a given soil (Cihlar, 1980c).

3. RESULTS AND DISCUSSION

3.1 Qualitative Analysis

HCMM transparencies showed a variety of effects caused by both meteorological and land surface parameters. These effects are discussed below for nighttime and daytime scenes over the western site from various dates.

3.1.1 Nighttime Imagery

Following an examination of all nighttime data, several scenes were found which were relatively cloud-free and covered southern Alberta (plains and the Rockies) and sometimes adjacent U.S. areas (Table 3). No nighttime data were available for this area outside the time period given in Table 3. The tones on the six images are roughly comparable because the mean temperature range (CR maximum - CR minimum Contrast Range values) was 17.5°K (standard deviation 3.3°K) and standard deviations of the CR minimum and CR maximum limits were 1.8 and 2.8°K, respectively (Table 3).

Date	Figure	Minimum Air Temperature (K)
19 May	5a	3.9 ± 2.3
20 June	5b	4.5 ± 1.3
30 June	5c	12.1 ± 1.0
22 July	5d	10.2 ± 1.5
29 August	5e	6.6 ± 1.3
9 October	5f	1.5 ± 2.1

An overview of the six nighttime images (Figure 5a through 5f) indicated that except for the 30 June image, the nighttime images selected over the western site exhibited low apparent temperatures and fairly complex thermal radiation patterns. To determine causes for these variations, the images were visually compared with

TABLE 3

Representative Nighttime HCMM Scenes Recorded Over Southern Alberta in 1978

Date of 1978	Centre Coordinates		I.D.	Contrast Range (CR)(°K) Values	
	Latitude	Longitude		Min.	Max.
19 May	51°43'N	114°11'W	A-A0023-10120-3	261.8	276.6
20 June	51°58,N	114°46'W	A-A0055-10100-3	260.5	278.9
30 June	47°59'N	113°22'W	A-A0065-09570-3	260.5	281.8
22 July	53°23'N	114°02'W	A-A0087-10040-3	264.9	282.5
29 August	50°07'N	110°03'W	A-A0166-09360-3	263.6	276.2
10 August	50°38'N	107°33'W	A-A0106-20180-2	262.2	311.7

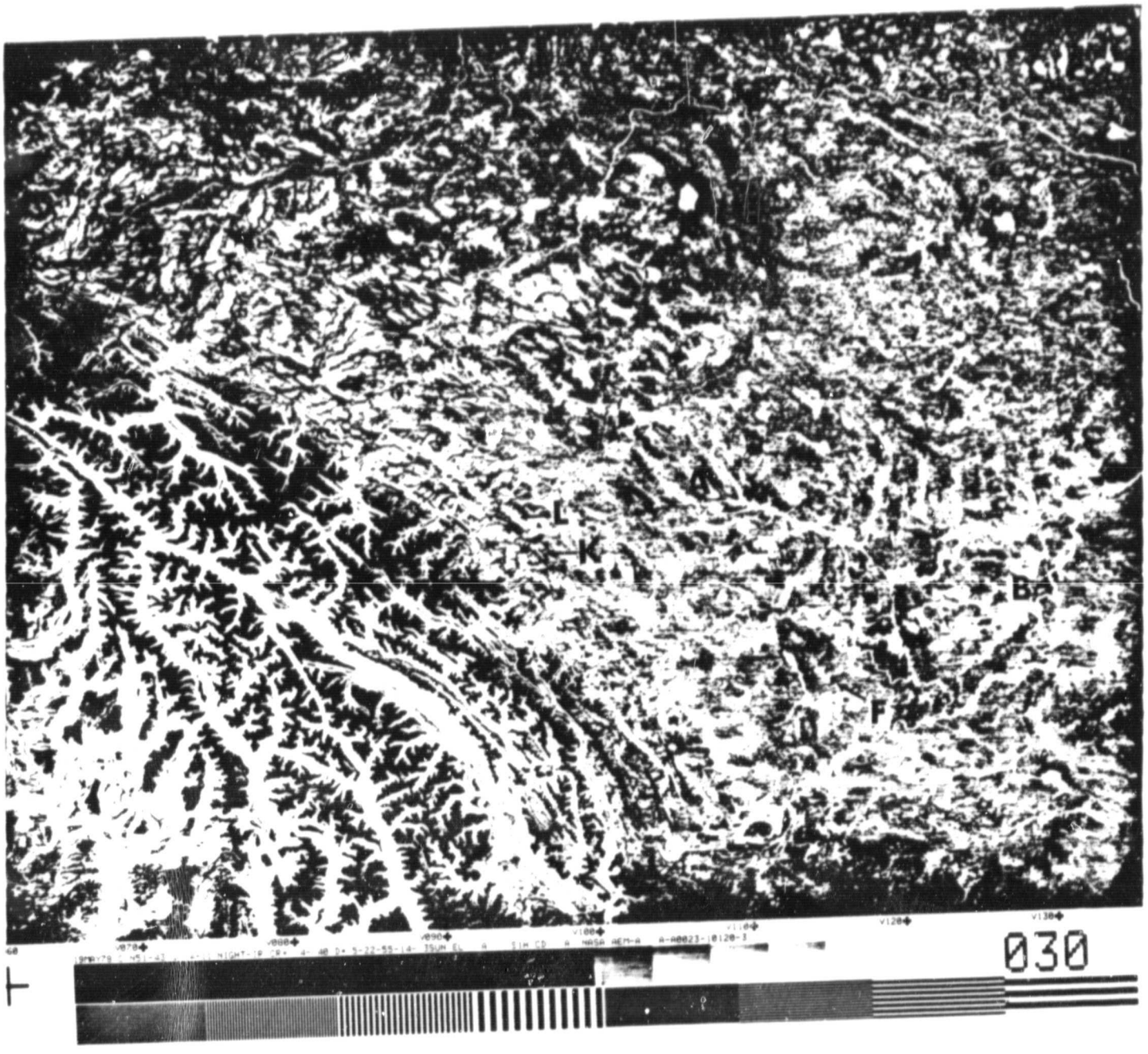

FIGURE 5a: Nighttime HCMM thermal infrared image over Southern Alberta acquired on May 19, 1978.

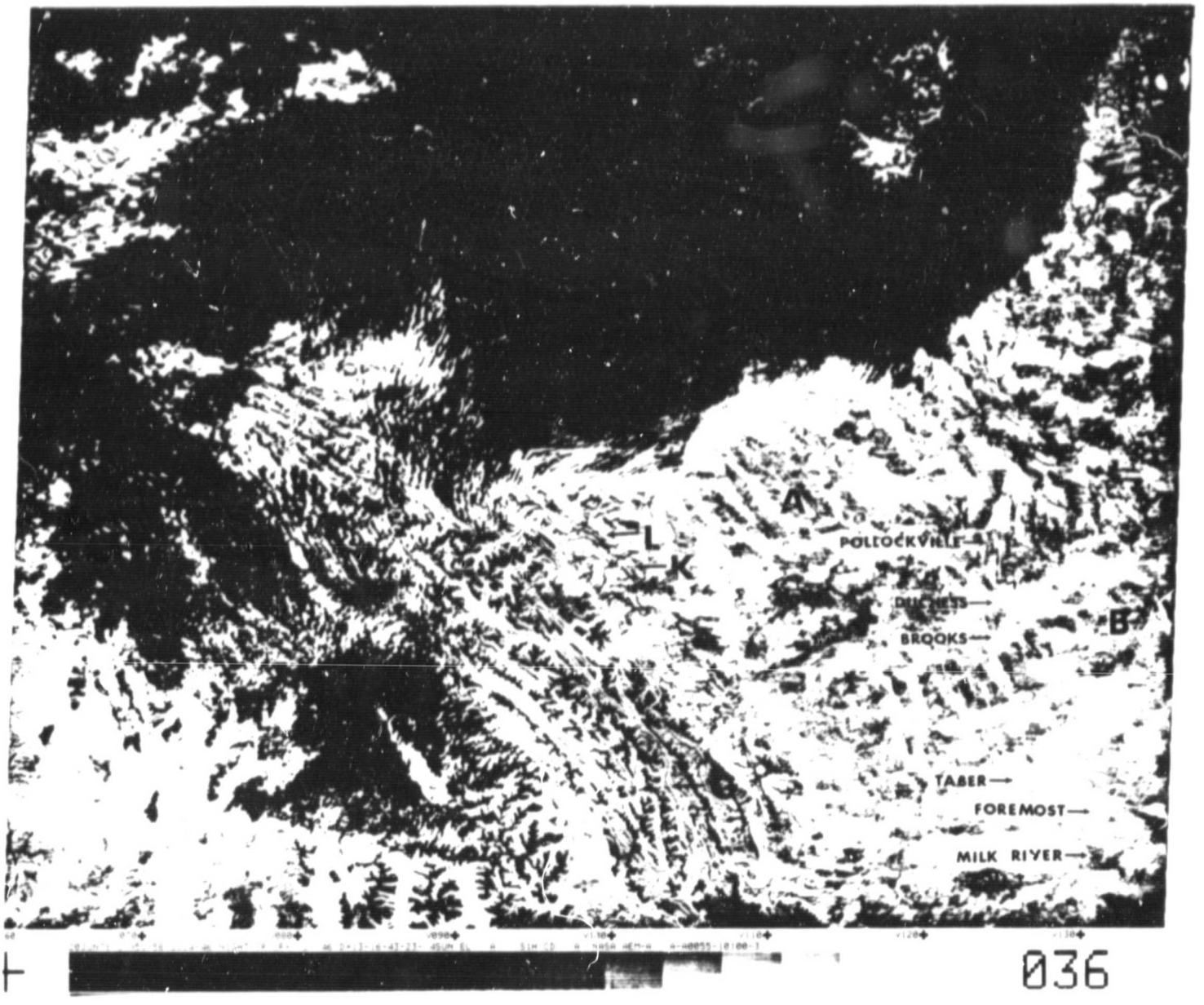

FIGURE 5b: Nighttime HCMM thermal infrared image over Southern Alberta acquired on June 20, 1978.

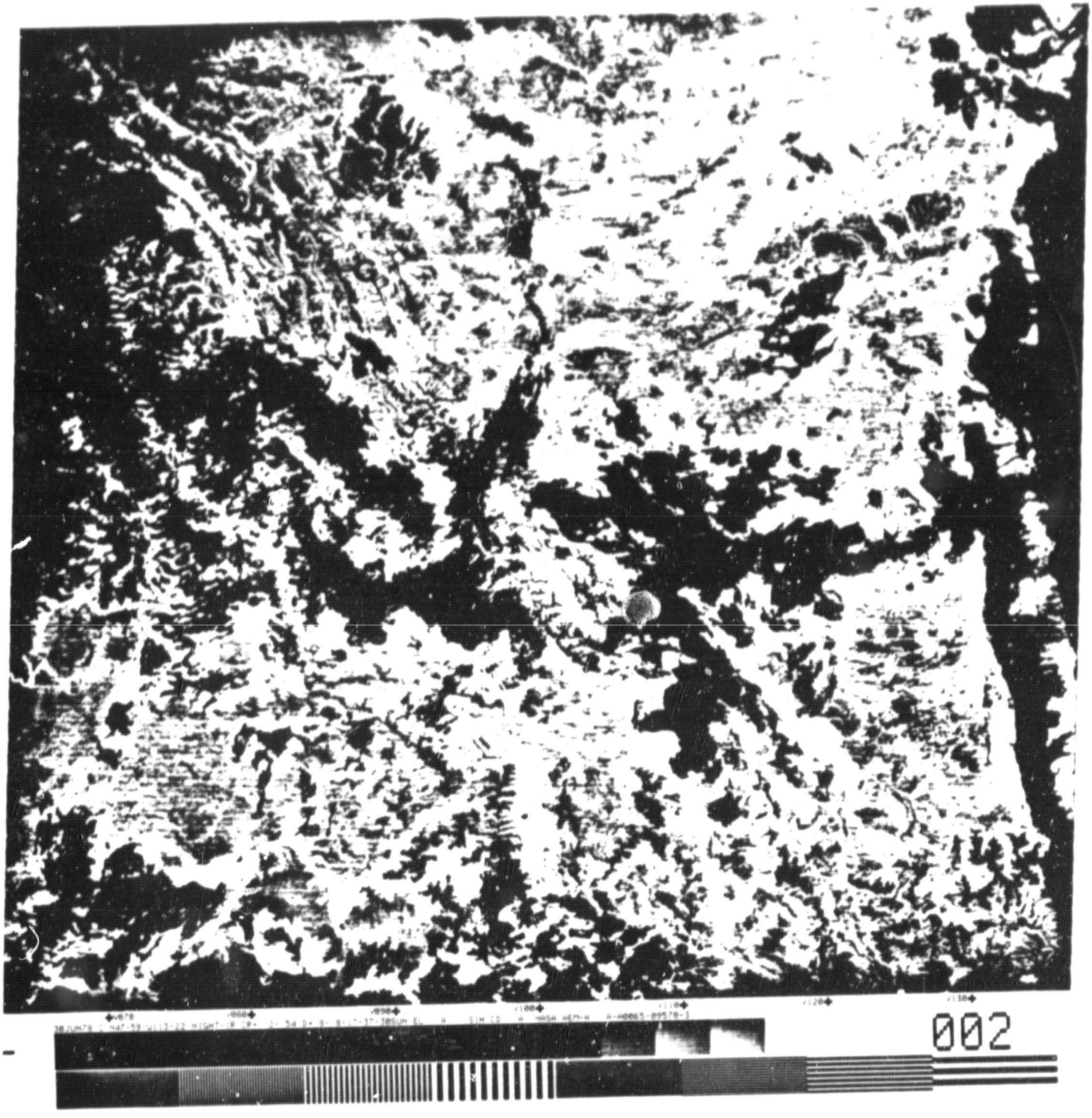

FIGURE 5c: Nighttime HCMM thermal infrared image over Southern Alberta acquired on June 30, 1978.

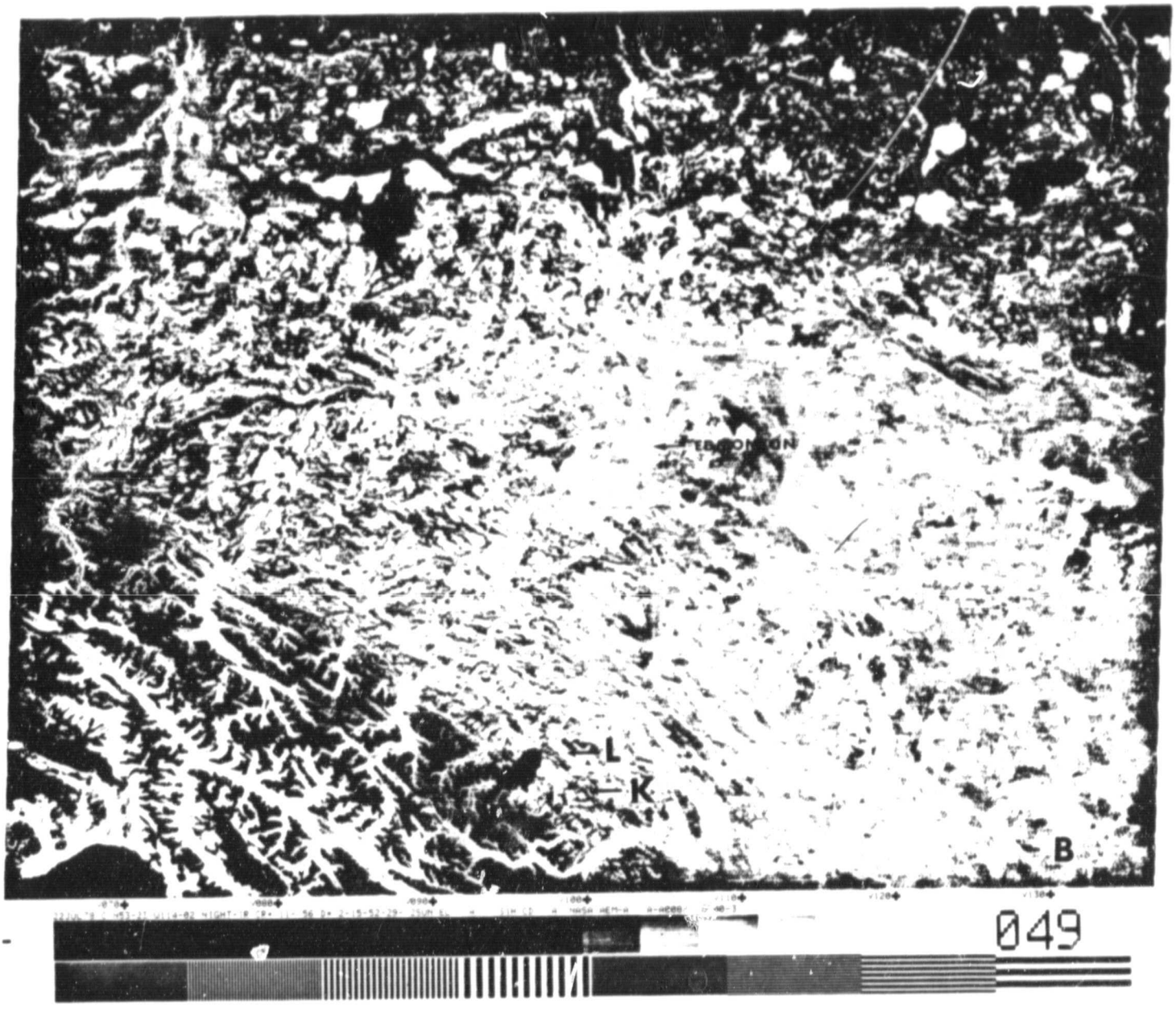

FIGURE 5d: Nighttime HCMM thermal infrared image over Southern Alberta acquired on July 22, 1978.

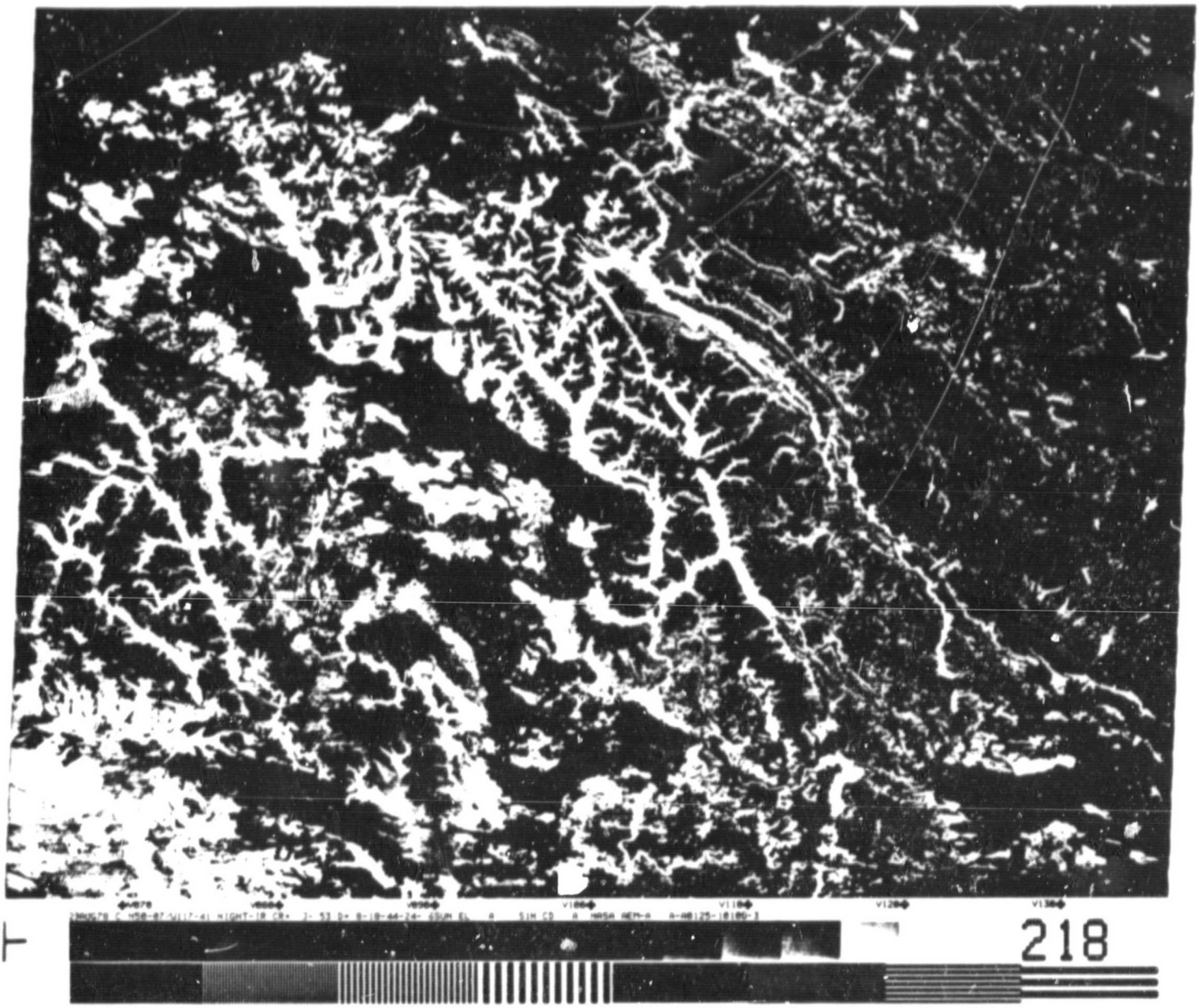

FIGURE 5e: Nighttime HCMM thermal infrared image over Southern Alberta acquired on August 29, 1978.

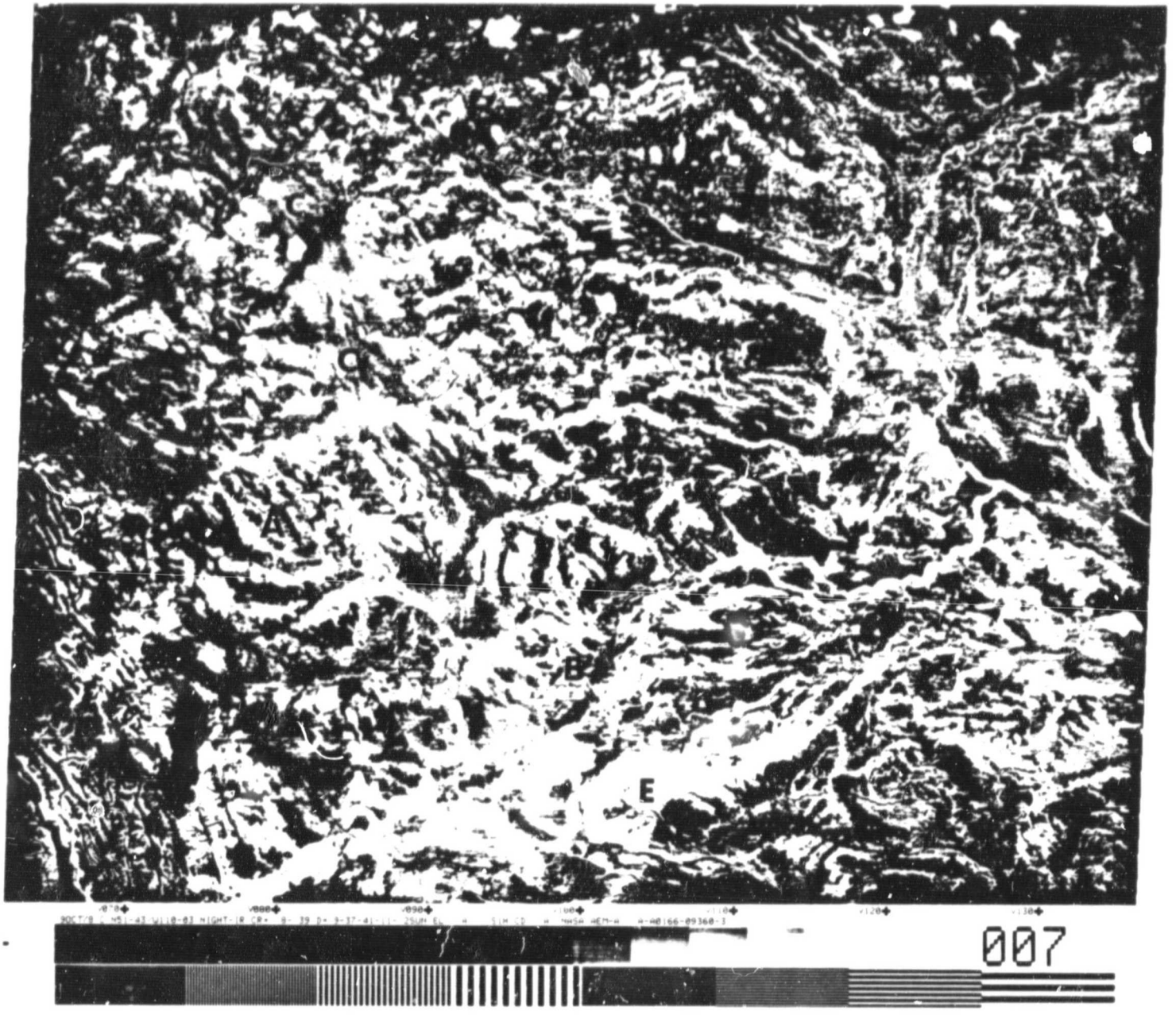

FIGURE 5f: Nighttime HCMM thermal infrared image over Southern Alberta acquired on October 9, 1978.

topographic, surface cover, geologic, vegetation, and other maps. It was concluded that the patterns in the plains corresponded generally to topography (Figure 6), but this relationship was not always well defined. For example, the ridges and valleys north of Calgary between Red Deer River and Kneehills Creek (A, Figure 5a) are visible in Figure 5b, 5e, and 5f; the valley to ridge-top difference is about 150 m in this area. On the other hand, most areas show thermal radiation patterns which varied between dates to greater or lesser extent. Note, for example, the appearance of the area between South Saskatchewan and Red Deer Rivers (B, Figures 5a, 5b, 5d, 5f). Some images show rather diffuse thermal patterns (e.g., Figure 5b), while others are quite distinct and sharply delineated (Figure 5f). This difference can even be observed in one image with similar topography (e.g., compare H and J in Figure 5a). Some patterns have regional extent (C, Figure 5f). While generally higher apparent temperatures in the plains correspond to higher altitudes, the reverse is sometimes the case. For example, Cypress Hills were colder on 9 October, 1978 than the surrounding land (D, Figure 5f) even though they rise about 600 m above the surrounding landscape. The warmer area NW of Cypress Hills is quite flat (E, Figure 5f). In areas of smaller altitudinal contrasts, thermal patterns may show a total lack of correspondence to topography (e.g., F in Figure 5a).

Given the thermal tone reversals discussed above, it appears that surface temperature distribution in the plains was influenced primarily by atmospheric variables, particularly near-surface air temperature and wind speed which affect the energy balance of the surface. To test this hypothesis, a regression analysis was carried out by relating apparent surface temperatures at 10 different dates to minimum air temperatures and wind speeds measured near the time of HCMM overpass at nine meteorological stations in southern Alberta. Figure 7 shows a plot of (i) air temperatures measured at the time of overpass for ten dates and (ii) minimum air temperatures for two dates against nighttime apparent temperatures; the apparent temperatures were obtained from optical transparencies (case (i)) and from digital data (for (ii)). The regression equation, computed only for data in (i), shows a close correspondence of HCMM and air temperatures ($r = 0.86$), particularly for lower air temperature values. No regression equation was computed for set (ii) because the HCMM and ground measurements did not coincide in time. However, one would expect that the apparent temperatures would be higher because the overpass took place before minimum temperatures were reached. This occurred only at one of the two dates, when air temperatures were high. For the other date (air temperatures 4 to 10°C), the relationship followed closely that obtained for set (i) (Figure 7). It is not clear why the air versus apparent temperature relationship was less accurately defined at higher air temperature values. However, since these values represent one date only (16 July), this result may not be representative. At air temperatures below 10°C, the relationship appeared sufficiently consistent to suggest the possibility of estimating near-surface air temperature from HCMM-type data with an accuracy (standard error of estimate) of approximately 2°C. In contrast to air temperature, wind speed values measured at overpass time were poorly correlated with the apparent temperature ($r = 0.21$).

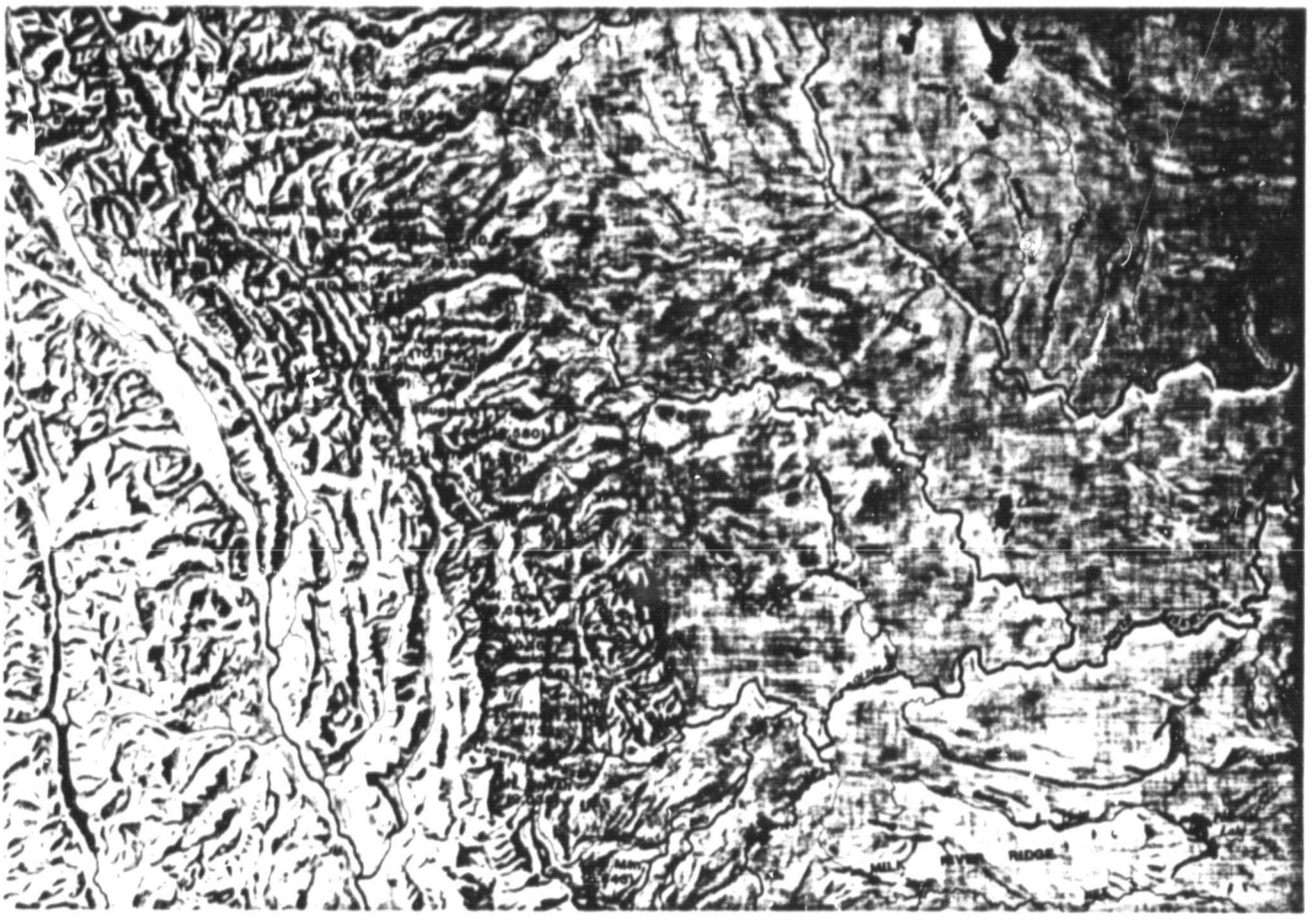

Figure 6: Physical features of southern Alberta. From: Atlas of Alberta, University of Alberta Press, Edmonton.

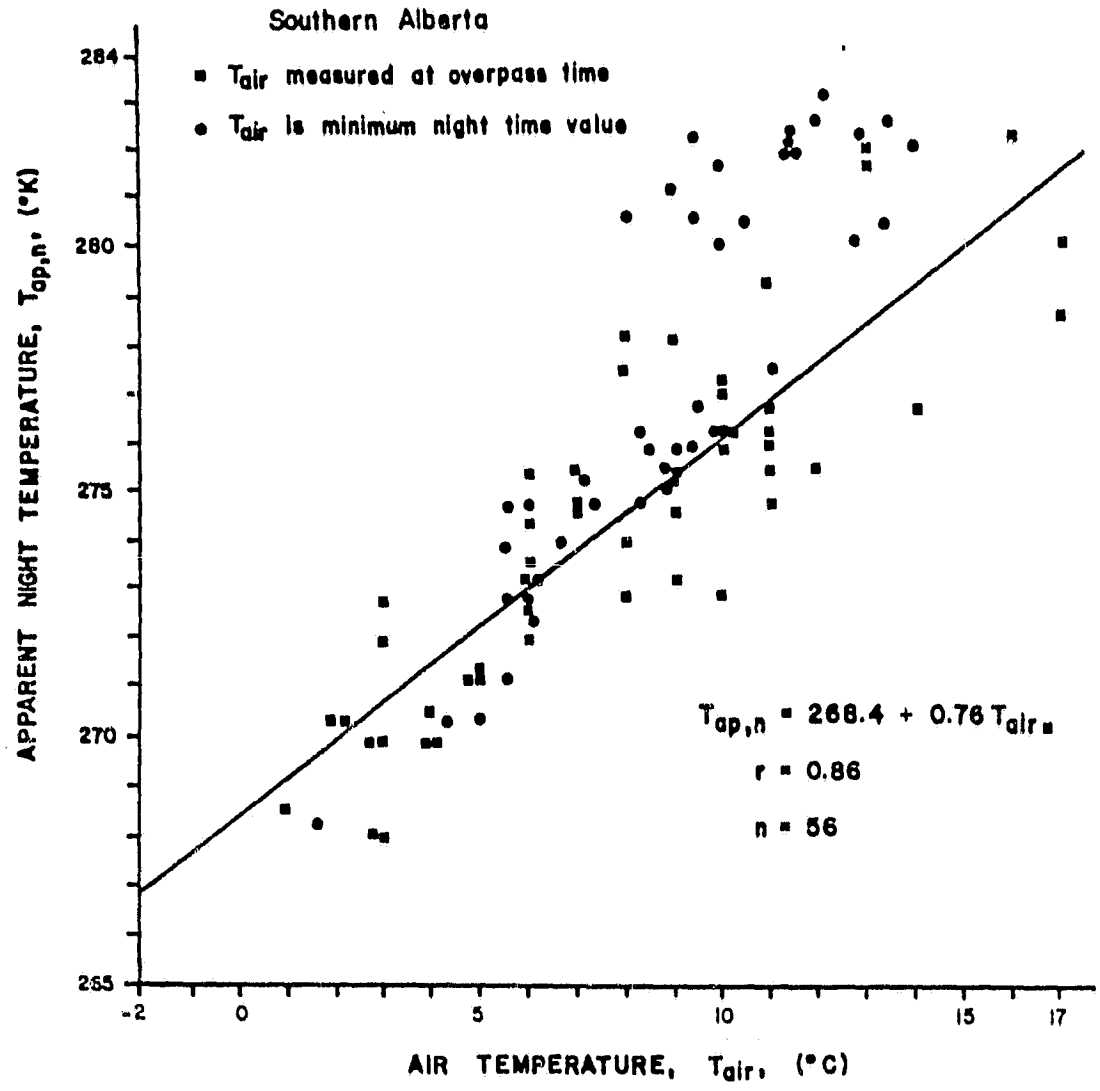

Figure 7: The relationship between HCMM apparent nighttime temperatures and air temperatures (i) measured at the time of overpass and (ii) minimum diurnal values. Data set (i) includes ten dates; set (ii), two dates.

The above results suggest that near-surface air temperature (influenced by altitude and wind-induced air mixing) is the primary factor determining the apparent surface temperature on cloud-free nighttime HCMM images.

In the Rocky Mountains, nighttime apparent temperatures were closely related to topography. The thermal patterns could be correlated with altitude, higher locations corresponding to lower temperatures. However, the valleys appeared much broader on the thermal images than in reality (e.g., Figure 5a vs. 6). It is evident that at higher altitudes, the apparent surface temperature was lower because of the lower air temperature, and for the same reason the apparent temperature increased with decreasing altitude. This does not explain, however, the lower apparent temperatures in the valley floors. Thermal emission in this area is probably due to the surface being cooled by radiation and by cold air drainage from higher elevations. A warmer, vapour-saturated air higher above the valley floor (e.g., fog) could be a contributing factor. The exact temperature values would then depend on local meteorological and topographic conditions. This explanation accounts for the apparent temperature maxima located between valley floors and ridge peaks which were observed on all nighttime images in Figure 5. It also implies that the maximum temperature isotherm would shift during the night as well as between dates; the latter can be observed in Figure 5 (G in Figure 5b vs. 5c).

The transition between the plains and the mountains occurs in the foothills where the nighttime effect of rugged topography is gradually less evident as one proceeds towards the plains. On some images (e.g., Figure 5a, 5b, 5e), a pattern of dark (cold) lines appeared which ran parallel to the mountain range. These lines always occurred at the same locations and could again be related to topographic variations, although they at first may seem to be superimposed over the topography (K, L in Figure 5a, 5b, 5d, 5e).

Land surface cover seemed to have litle effect on the nightime thermal patterns. Water in lakes had a very different temperature, and rivers could also be traced although their contrast with adjacent land was lower in many cases compared to the larger lakes. Evidently, the HCMR spatial resolution relative to size of the water bodies, and land/water temperature differences determined the resulting thermal contast. In the plains, the effect of land surface cover could not be detected on images shown in Figure 5. This was true even for distinctly different cover types such as irrigated land and rangeland. Urban heat islands could be detected (e.g., Edmonton in Figure 5d); however, this seems to be primarily due to anthropogenic heat and not because of surface cover.

Although the above effects and trends were illustrated only on a few images, they are consistent with those observed on numerous other nighttime images covering this geographic area.

3.1.2 Daytime Imagery

Daytime reflectance (0.5 to 1.1 micrometres) images were generally sharper because of a better HCMR spatial resolution in this spectral band but also had considerably narrower optical density range for land surface features. While moderate or heavy clouds were always prominent (Figure 8b), on land only green vegetation had a distinctly different albedo. For this reason, and since better satellite data in this spectral band are already available from the Landsat series, the HCMR reflectance band data were not analyzed in detail.

Several relatively cloud-free images were selected to examine seasonal variations and parameters important for the daytime HCMM thermal images (Table 4 and Figures 8a through 8g). These images depict primarily areas east of the Rockies because practically all daytime thermal infrared images received over the Rockies had an excessive cloud cover. An examination of other images for mountainous areas on the eastern and western sites indicated that altitude had a strong effect on apparent daytime temperatures in the absence of clouds, particularly if large altitudinal differences are involved. This is to be expected given the predictable air temperature decrease with altitude.

The most striking feature of all daytime thermal images of the western site is the heavy cloud cover. The images shown in Figure 8 were selected because of their low cloud cover over southern Alberta but even these areas are frequently obscured. Besides complete obliteration of the ground signal caused by moderate or heavy clouds apparent on the reflectance band data, surface emission was often appreciably attenuated through the presence of a non-visible cirrus layer. Since these layers are not evident on the reflectance band images (Figure 8b vs. 8c), atmospheric attenuation (and not the reduction of incident radiation) must be the primary cause of lower apparent temperatures. The ground signal attenuation varies from low values to 100% and the limits of areas with ground thermal radiation modified in this manner are usually very difficult to identify. In other words, it is difficult to separate atmospheric effects from surface effects. The effects of sub-visible clouds can sometimes be established from their adjacency to visible clouds (A, Figure 8e, 8f) or from spatial orientation (B, Figure 8d, 8e). These aids are often absent, however. For example, areas C (Figure 8c) are not clearly related to any cloud formation. They occur over large areas and might also represent recent precipitation. The problem is further complicated by topography and ground cover. For instance, D (Figure 8c, 8d) are hills covered with trees and E (Figure 8c) also represents a topographic effect. The most reliable visual clues to detecting severe atmospheric attenuation in this region seems to be the presence, within an image, of areas with high apparent surface temperatures (light tones; e.g., Figure 8e) and of sharp contrasts between adjacent cover types known to have different surface temperatures: land vs. water, irrigated area vs. rangeland (F, Figures 8c, 8d). Surface cover contrast is less reliable because of seasonal temperature changes (F, Figures 8a, 8g). Atmospheric

TABLE 4

Representative Daytime HCMM Thermal Infrared Scenes Recorded Over Southern Alberta During 1978

Date of 1978	Centre Coordinates Latitude	Longitude	I.D.	Contrast Range (CR)(°K) Values Min.	Max.
2 June	49°10'N	108°41'W	A-A0037-20340-2	260.9	320.5
15 July	49°10'N	108°41'W	A-A0037-20340-1	-----	-----
15 July	48°10'N	110°00'W	A-A0080-20350-2	262.2	312.5
10 August	50°38'N	107°33'W	A-A0106-20180-2	262.2	311.7
26 August	51°39'N	107°41'W	A-A0122-20150-2	261.3	301.9
28 September	47°45'N	115°58'W	A-A0156-20480-2	260.9	300.0
14 October	47°42'N	111°19'W	A-A0171-20280-2	263.3	294.9

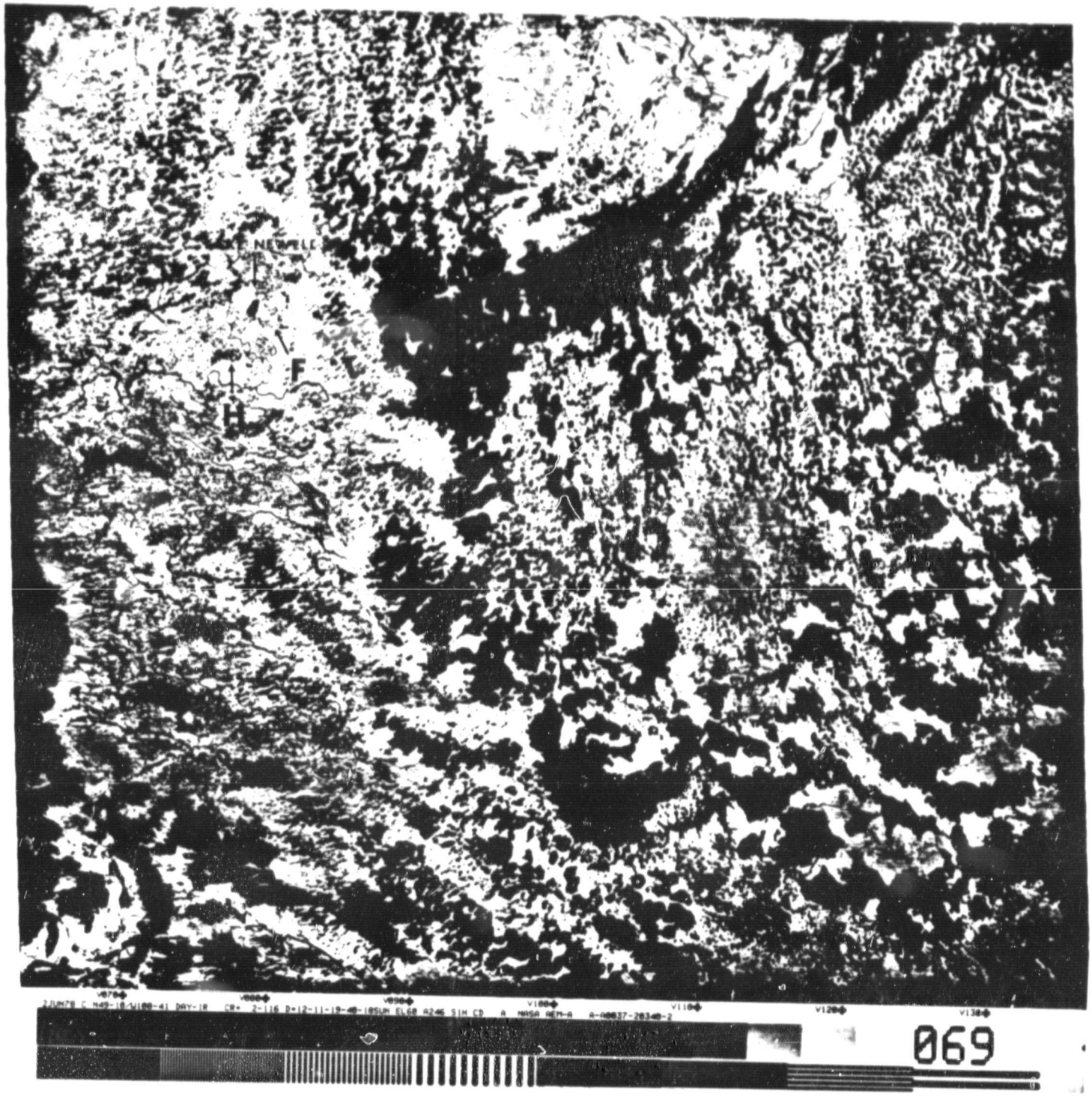

FIGURE 8a: Representative daytime image over Southern Alberta acquired on June 2, 1978.

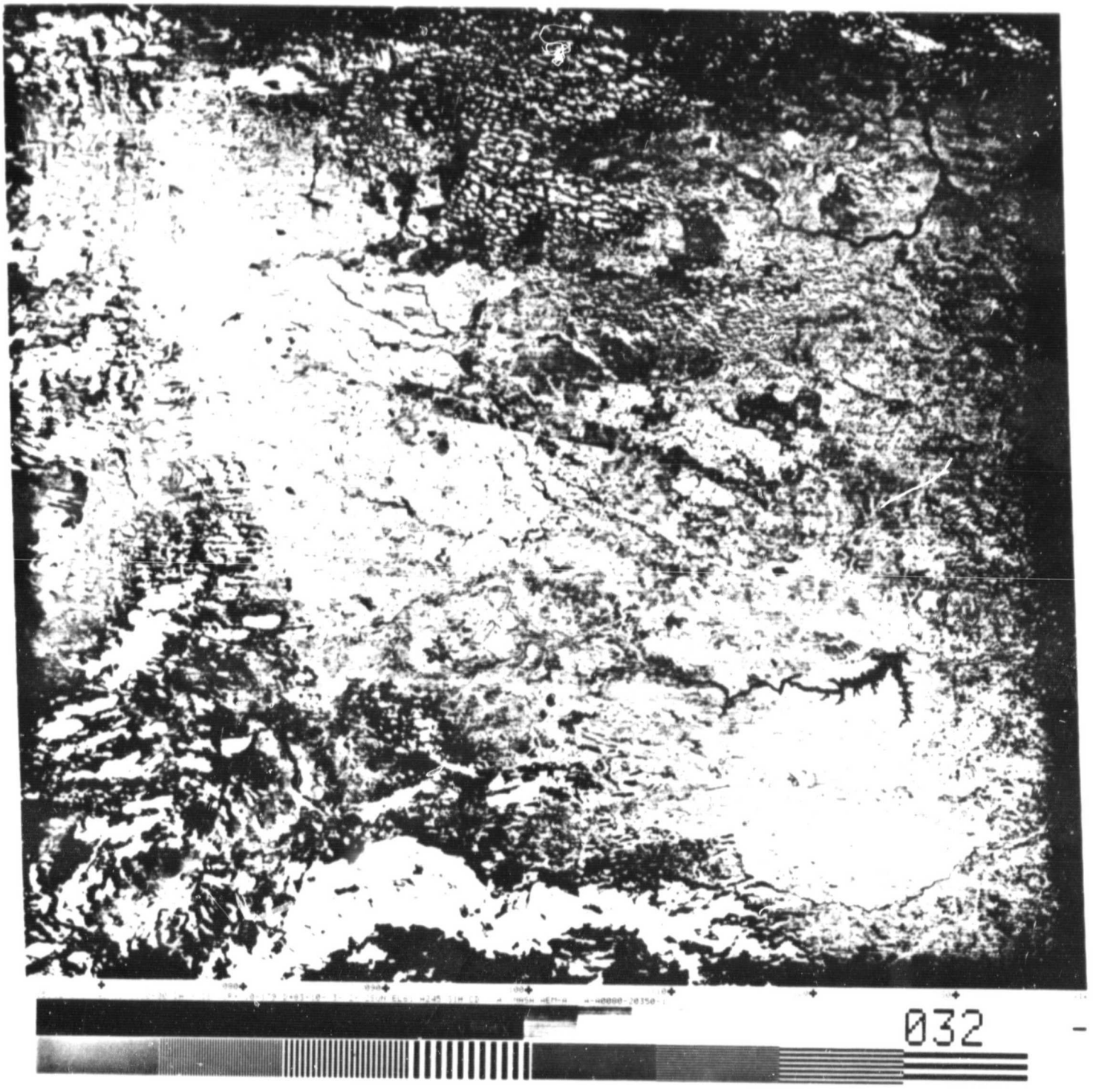

FIGURE 8b: Representative daytime image over Southern Alberta acquired on July 15, 1978.

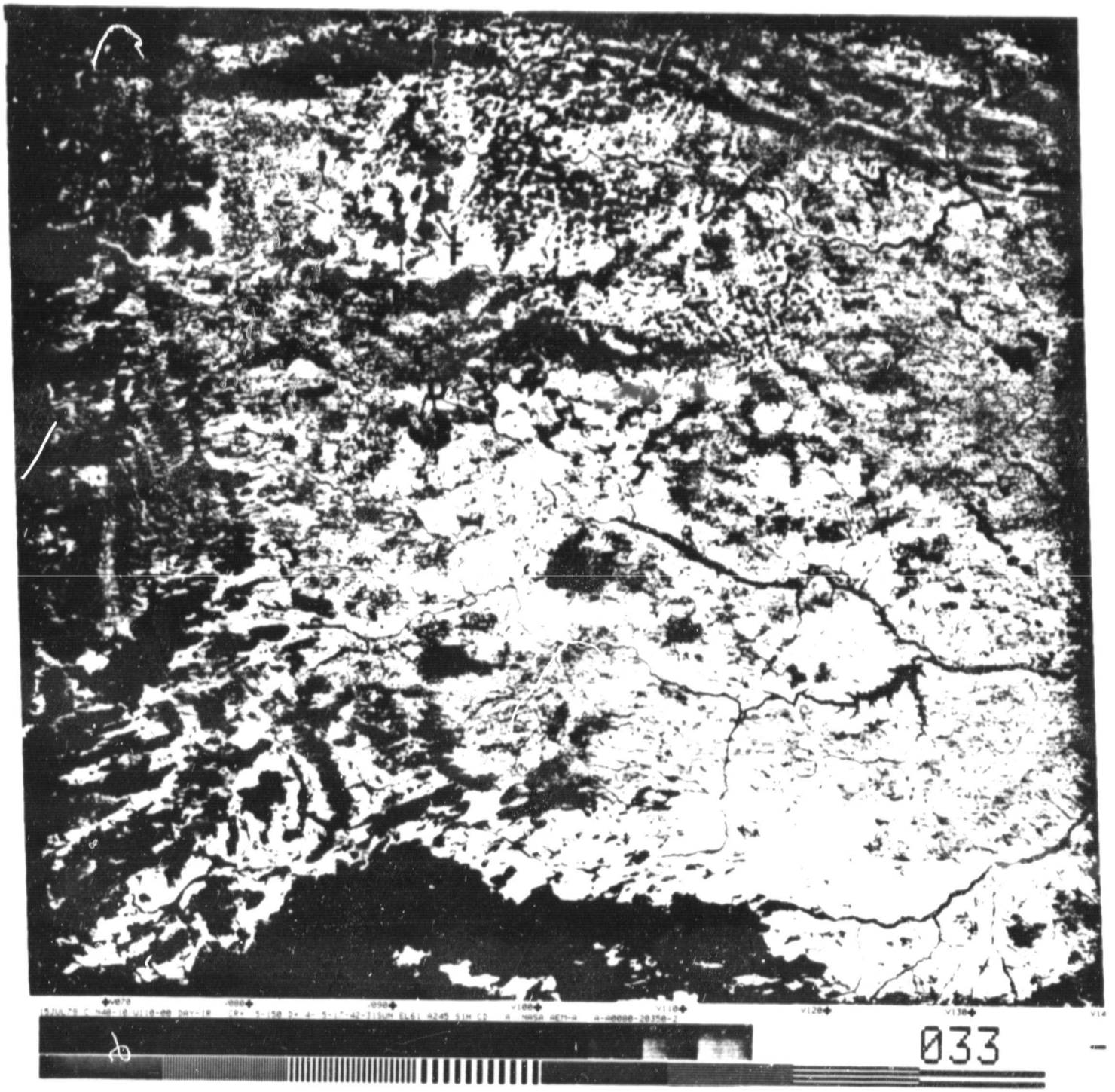

FIGURE 8c: Representative daytime image over Southern Alberta acquired on July 15, 1978.

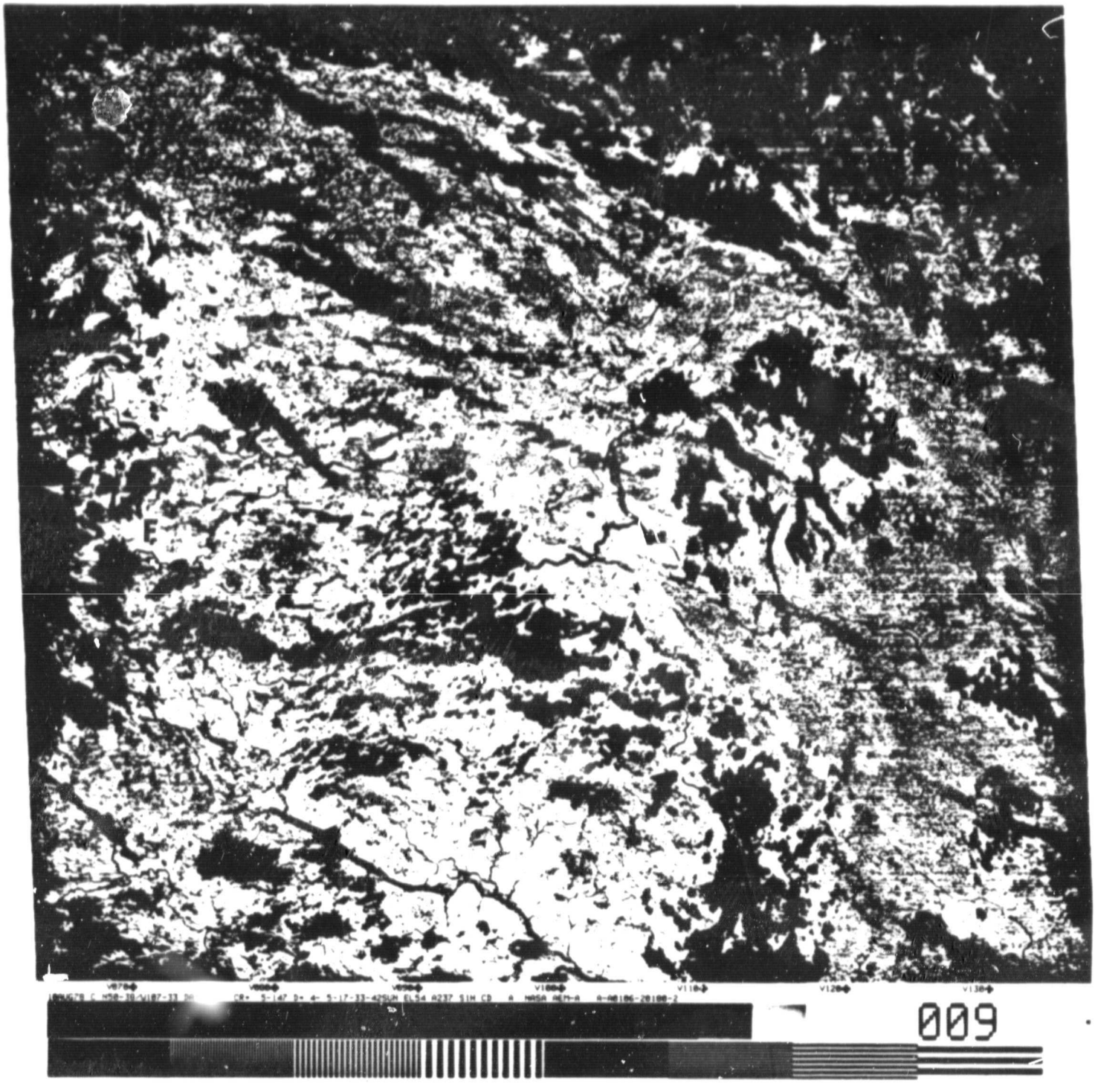

FIGURE 8d: Representative daytime image over Southern Alberta acquired on August 10, 1978.

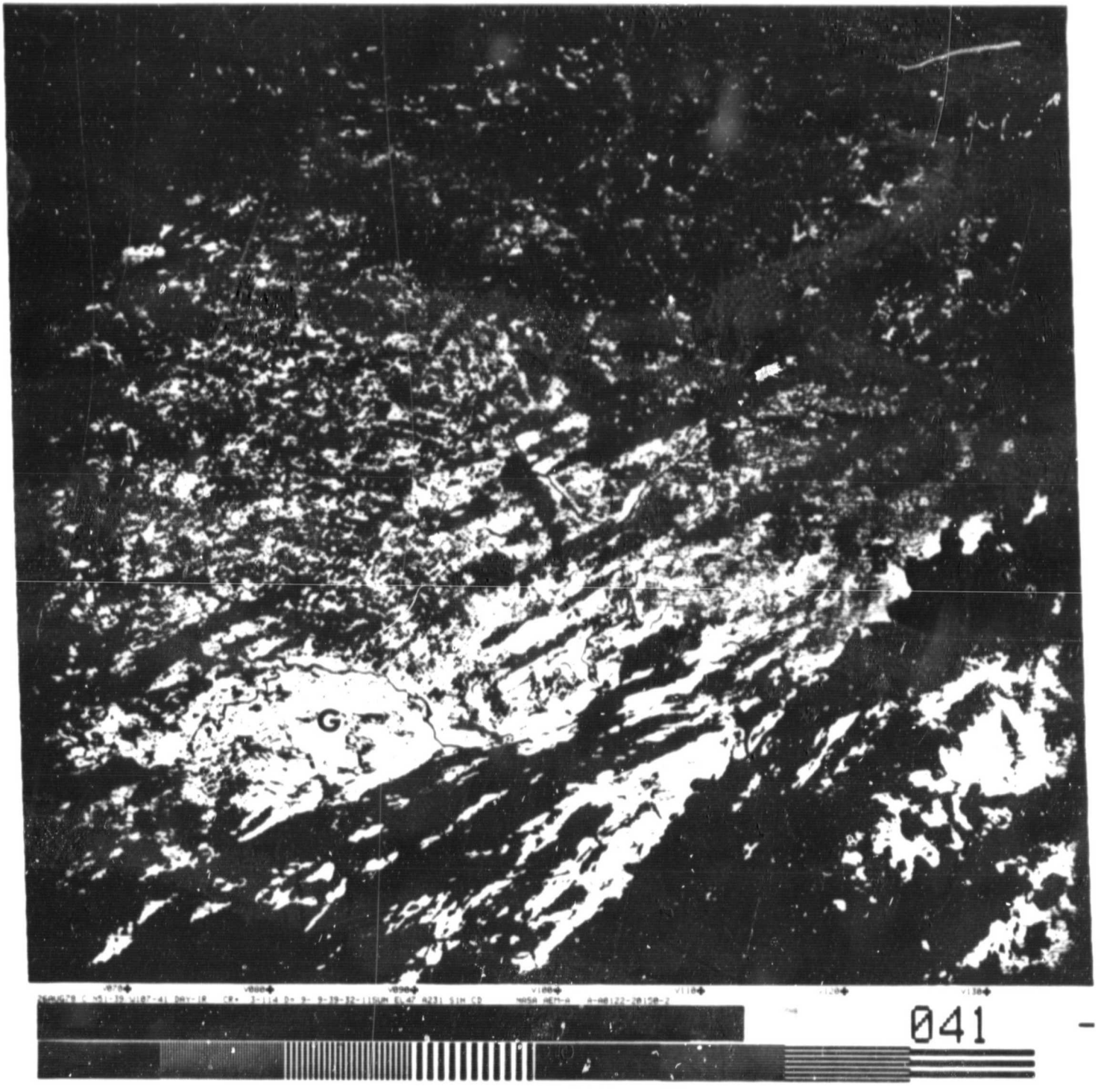

FIGURE 8e: Representative daytime image over Southern Alberta acquired on August 26, 1978.

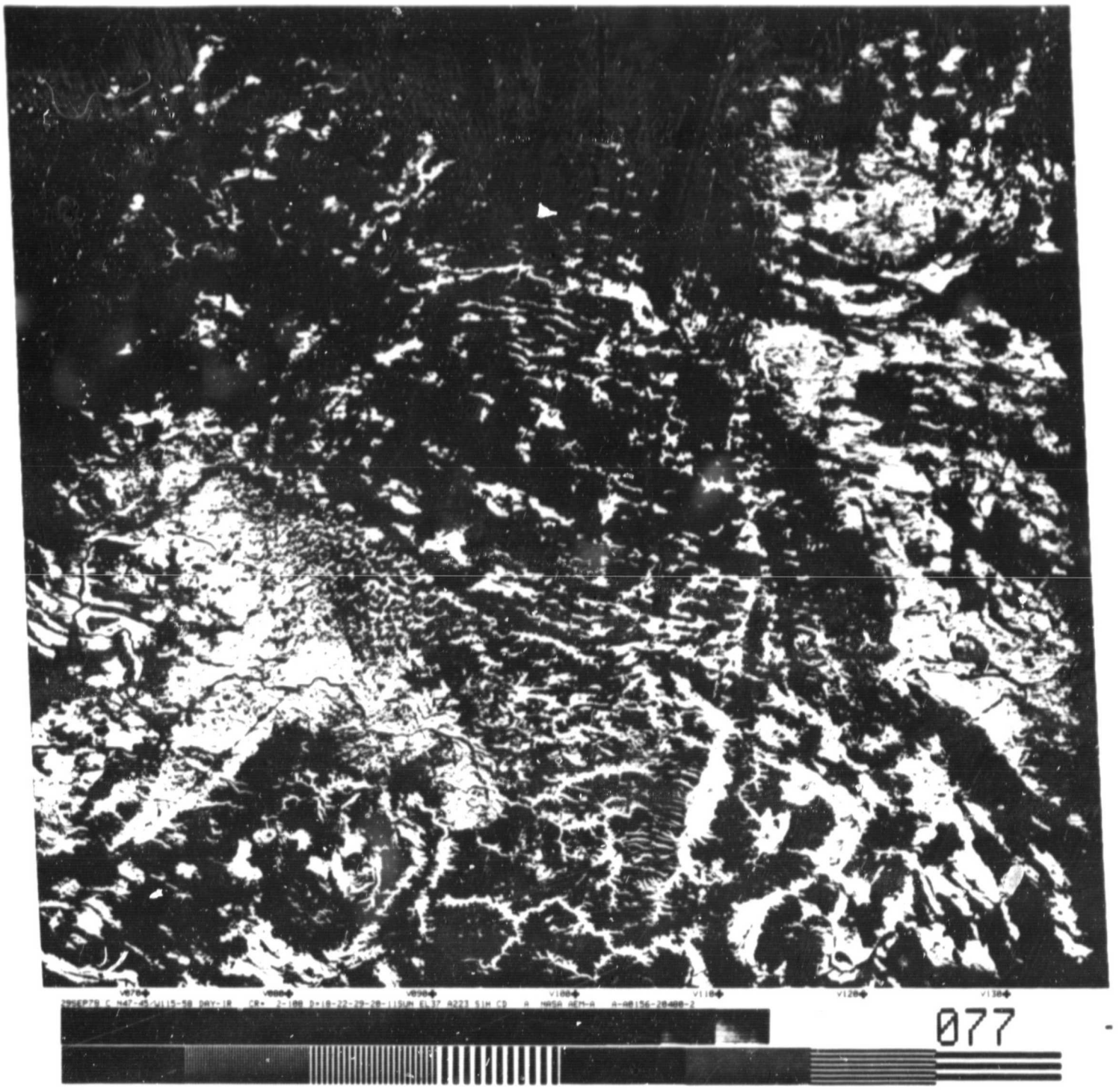

FIGURE 8f: Representative daytime image over Southern Alberta acquired on September 29, 1978.

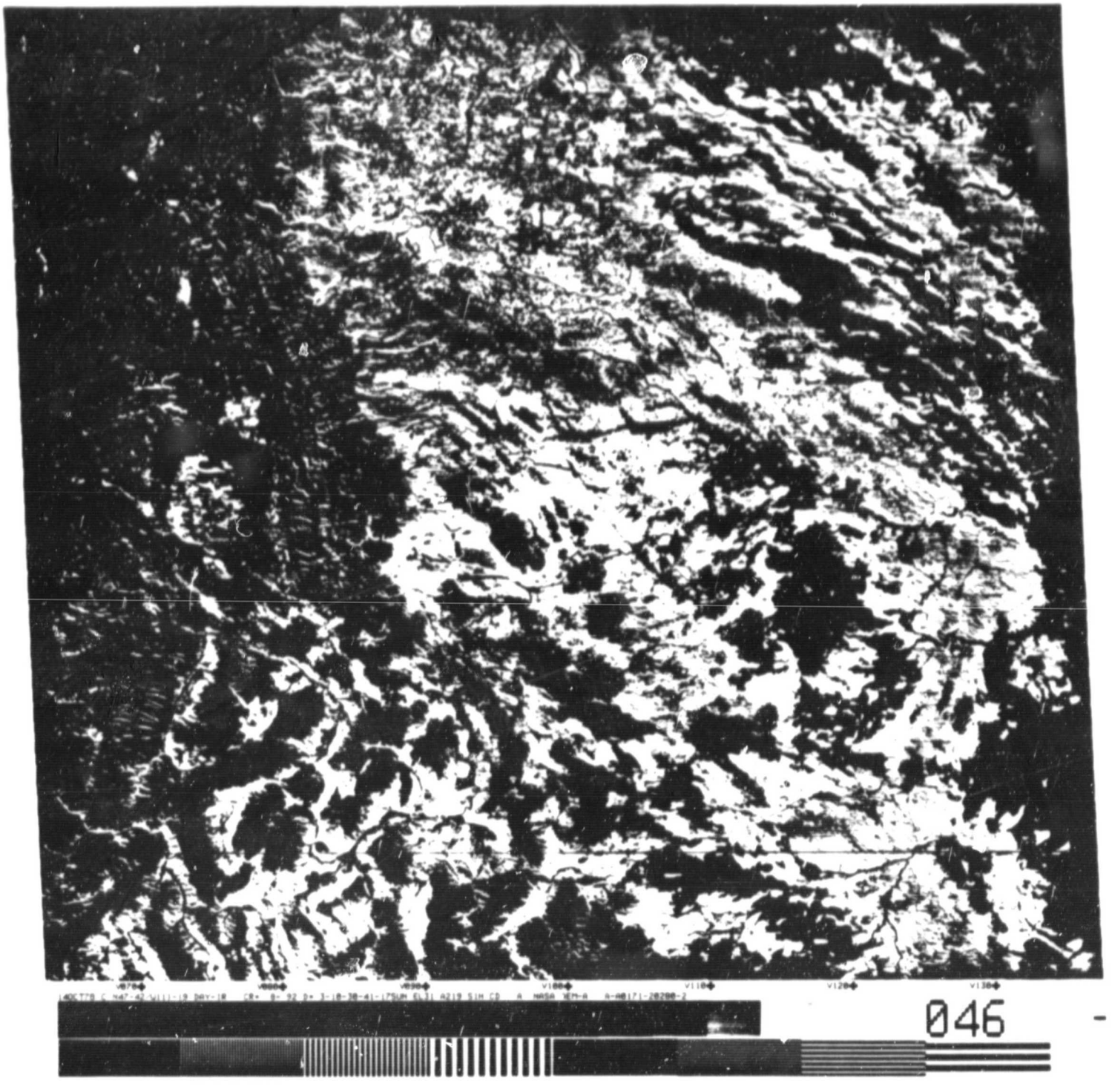

FIGURE 8g: Representative daytime image over Southern Alberta acquired on October 14, 1978.

attenuation reduces surface temperature contrasts over larger areas which may also help to differentiate surface effects (e.g., G in Figure 8e is a surface cover effect). The land/water contrast seems a more reliable indicator although the expected temperature contrasts for water and adjacent land surface cover types must be taken into consideration. For example, rangeland/lake thermal contrast should decrease from spring to summer. Since the contrast was larger for Lake Newell on 15 July, 1978 (Figures 6 and 8c) than on 2 June (Figure 8a), it would appear that atmospheric attentuation was stronger on 2 June in this area. Evidently, the optimum approach to detecting and removing atmospheric effects would be a remote sensing system which would permit doing this on a pixel-by-pixel basis.

Under clear sky conditions, surface cover was the most important variable affecting the amount of emitted thermal radiation. The highest contrast was observed between land and water, and secondly between "cool" irrigated cropland and "warm" rangeland (H, Figure 8c). Since rangeland in this area consists of mixed grass prairie with moderate to sparse ground cover and a large proportion (about 50% or more in July) of brown biomass, the temperature difference between the latter two surfaces must be attributed to high evaporative cooling and a good ground cover of the irrigated crops. Due to the phenological development of agricultural crops, the cropland/rangeland contrast varied during the season, it being strongest in July and decreasing in both directions (H, Figures 8a, 8g). Although numerous large circular pivots (160 acres and above) were present in the area around Lake Newell (Figure 8a), the HCMR resolution was not sufficient to properly show thermal variations within the irrigated area.

3.2 Quantitative Analysis

3.2.1 Effect of Surface Cover and Topography

To quantitatively assess the effect of surface cover on HCMM measurements, histograms for individual HCMM bands were extracted from the nearest neighbour data set for a number of areas with different land covers. The following categories were defined: water, rangeland, dry cropland, irrigated cropland, and cities. With the aid of Landsat images and aerial photographs, the training areas were located on the CIAS image display and were delineated by a cursor. The histograms were then determined through one-dimensional training for all bands. Daytime and nighttime apparent temperatures are shown in Figure 9 as means and standard deviations for two dates and several training sites at each date. Where the mean is joined by a line with the standard deviation limits, the calculations were performed on a sample of 390 pixels; the remaining training sites consisted of 39 pixels. Thus, for example, five training sites representing irrigated cropland were selected on the 14 June image, one 390 pixels and four 39 pixels in size. Water is not shown because the difference between day and night temperatures was very small there.

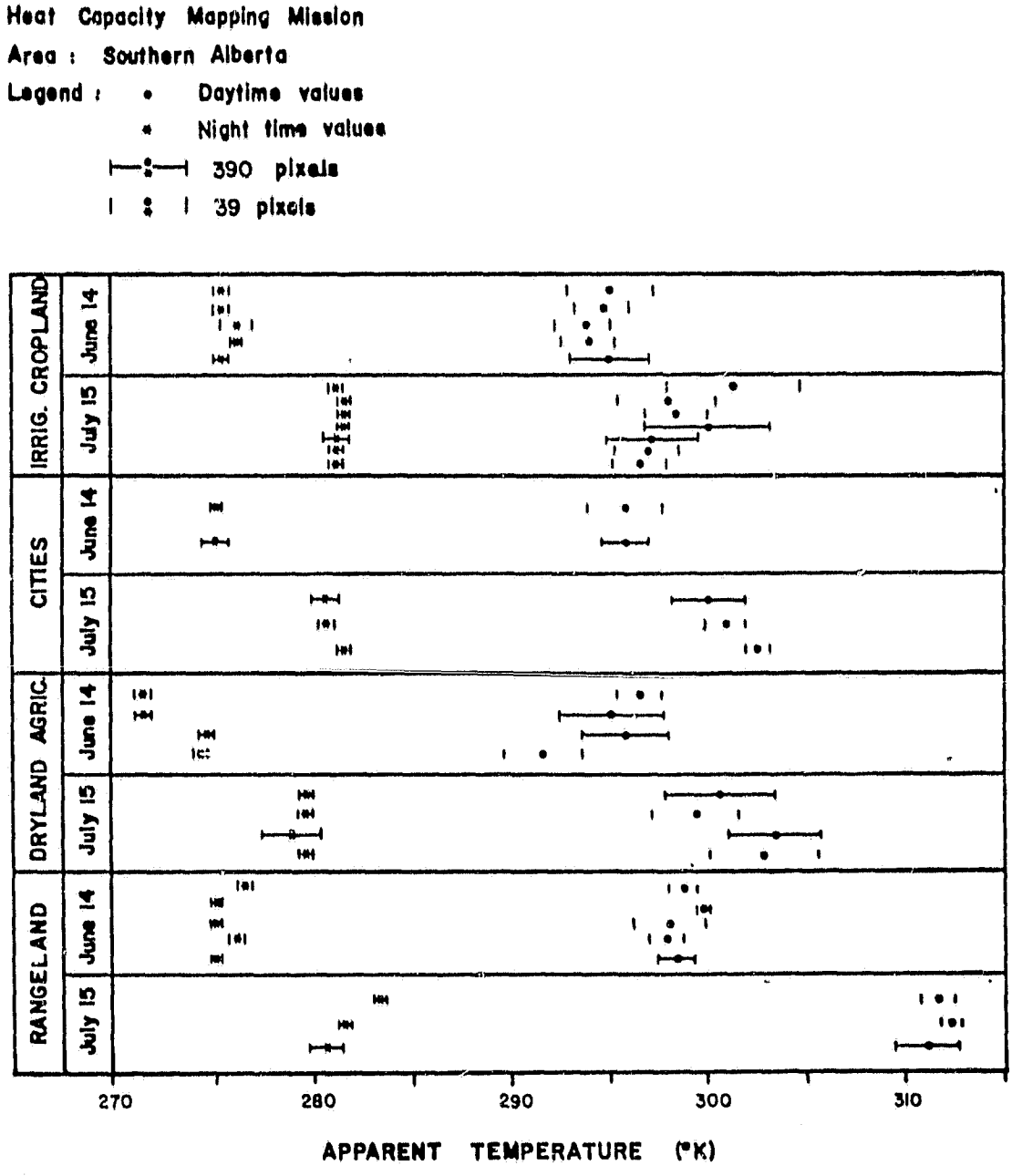

Figure 9: Nighttime and daytime apparent temperature distributions (mean, standard deviation) in southern Alberta for various land cover types and two dates, 14 June and 15/16 July.

An examination of Figure 9 shows several systematic trends. The range of nighttime temperatures for a given date was very narrow, both within and among cover types. There was a systematic shift of about 5°C between 14 June and 15/16 July nighttime data which can be attributed to air temperature (the average minimum diurnal air temperature of 26 stations in the area was 6.7°C and 11.5°C on 14 June and 16 July, respectively). Also, daytime temperature values were higher for 15 July compared to 14 June for all cover types; the difference ranged from about 3°C (irrigated cropland) to 13°C for rangeland. Moreover, daytime temperature histograms of a given cover type were broader than corresponding nighttime data (Figure 9). The average standard deviation was highest for dryland agriculture (2.2°C, both dates combined) followed by irrigated cropland (1.9°C), cities (1.4°C) and rangeland (1.3°C). These values were calculated by averaging within-training site standard deviations for each cover type. The decreasing order of cover types is related to increasing surface cover homogeneity. While rangeland areas were covered by a relatively uniform vegetation canopy, dryland agricultural areas included "cooler" crops and "warmer" fallowed fields thus giving rise to a broader temperature historgram. Similarly, irrigated croplands consisted of irrigated fields, non-irrigated fields, roads and built up areas. Cities have a variety of cover types but these vary at a high frequency and therefore create relatively homogeneous HCMM pixels.

Another observation concerns the day-minus-night apparent temperature difference ΔT. On the 14 June image, ΔT values ranged from about 19°C (irrigated cropland) to 22°C (rangeland). In July, the range was lower for irrigated cropland (17°C) but much higher for rangeland (30°C); ΔT values for cities and dryland agriculture were essentially the same as on 14 June (Figure 9). Based on the known seasonal trend of vegetation development, it is suggested that the differences between June and July ΔT values are primarily due to the changes in cover and vigour (transpiration rate) of vegetation. Both parameters decrease between June and July for rangeland but increase for the irrigated areas. Dry cropland behaved consistently with this hypothesis as it consisted of green crops with lower plant cover and a lower transpiration rate, and it included appreciable amounts of fallow fields and rangeland.

Means and standard deviations calculated for training areas of 390 pixels (Figure 9) were used to statistically test the differences between individual cover types. First, Student's t-values were computed separately for every pair of training sites for each date and time. With few exceptions, daytime and nighttime apparent temperatures were found to be significantly different between individual training sites at the 0.001 probability level. To compare the relative differences among land cover types, all pair t-values were summed for each cover type. For example, for the 14 June, 1978 daytime data, t-values in the case of rangeland were 33.8 vs. irrigated land, 31.3 vs. cities, and 24.3 vs. dryland agriculture, or a total of 89.4. The totals were then ranked with the assumption that the higher the total, the more "different" that cover type appears from the remaining ones. The following results were obtained:

14 June, 1978

Day: Rangeland > Irrigated land > Cities > Dryland

Night: Dryland > Irrigated land > Rangeland > Cities

15 July, 1978

Day: Rangeland > Irrigated land > Cities > Dryland

Night: Dryland > Rangeland > Irrigated land > Cities

It is worth noting that the daytime rank orders were identical for both dates, and the nighttime ranks were also very similar. In the daytime data, rangeland had a much higher total t value than the remaining three types which were more similar. At night, the total t values were more uniformly distributed, with dryland agriculture showing the highest value. On both dates, this cover type was the coldest at night. It is suggested that the rank order stability was partly due to effects other than surface cover, such as altitude and atmospheric effects. The training sites representing individual cover types were the same on both dates. The dryland agricultural site was located at a higher altitude and this could be the reason for its lower apparent nighttime temperature. Furthermore, the pairs of irrigated and dryland sites measured on 15 July, 1978 were significantly different within the cover type.

From the viewpoint of the feasibility of soil moisture estimation, it should be noted that for any land cover type (training site) except cities, soil moisture or plant stress effects are included in the scatter of points about the mean value which is described by the standard deviation. For areas fed only by precipitation (rangeland and dry cropland) and assuming normal distribution, 95% of the observed daytime apparent temperature values would be within a range of about 7° (±2 standard deviations) at each date. This value was obtained by averaging standard deviations for all rangeland and dry cropland training sites, separately for each date (9 cases for 14 June, 7 cases for 15 July).

The relative effects of surface cover and topography are illustrated in Figure 10 which represents a 70km long NW transect from the plains to the Rockies. Nighttime thermal IR data were fairly closely related to topography, particularly where large topographic differences exist. Daytime temperature values responded to surface cover but due to the early stage of crop development, only surface water locations are distinct. The effect of large altitudinal variations is also shown in the daytime image even though less clearly than in the night data. Figure 10 thus shows that topographic and surface cover both influenced the daytime apparent temperatures measured by HCMR and that either one can assume prime importance. Where topographic variations are not large (as in the prairies), surface cover was more important of the two.

3.2.2 Effect of Soil Moisture

To determine if a relationship exists between HCMM measurements and soil moisture, digital satellite data were extracted for meteorological station locations and surrounding areas. Data from 14 June and 15 July, 1978 for the western site and those from 6 June, 1978 for the eastern site were used. Digital data were extracted from all HCMM bands for 15 July and 6 June, and from Landsat data for 22 June. Only daytime data were used for 14 June because of the failure by NASA or CCRS to accurately register the day and night HCMM data.

The Antecedent Precipitation Index (API) was selected as a compromise measure to describe the soil water status. As indicated in Section 1, the emitted thermal IR radiation is related to moisture content of the surface layer, the root zone, or a mixture of the two depending on the degree of plant cover. However, HCMM resolution was not sufficient to separately image different fields, thus mixed pixels including various crops/plant cover levels were present in most cases. In addition, their proportions differed at the three dates studied. Given these ambiguities, it was decided to use the API which reflects primarily the near-surface moisture status and which has been successfully used in previous soil moisture detection studies employing satellite data (McFarland, 1976; McFarland and Blanchard, 1977; Schmugge et al, 1977). The API values were calculated for each target date and meteorological station. The satellite data (extracted from the pixel in which the station was located and converted into albedo and apparent temperatures following procedures described by Anonymous (1978)) and API calculations were then entered into computer and an analysis was carried out.

It was found that API calculations for the various k values were closely correlated. As an example, correlation coefficients for the western site, 14 June 1978 data are given in Table 5. For the subsequent analysis, values calculated with $k = 0.85$ were therefore chosen. This value is higher than that used by McFarland and Blanchard (1977) for comparable seasonal periods, but their data were obtained at much lower latitudes.

A plot of API vs. daytime apparent temperature showed several anomalous points with very low temperature values which were found to be located in areas covered by clouds during the daytime HCMM overpass. These stations were therefore excluded from the subsequent analysis. Correlation analysis was then carried out for the following data subsets:

(i) all meteorological stations not obscured by clouds on the NN (nearest neighbour) - resampled image (6/6, 14/6, 15/7);

(ii) all meteorological stations shown on NN and CC (cubic convolution) - resampled images and not obscured by clouds (14/6, 15/7);

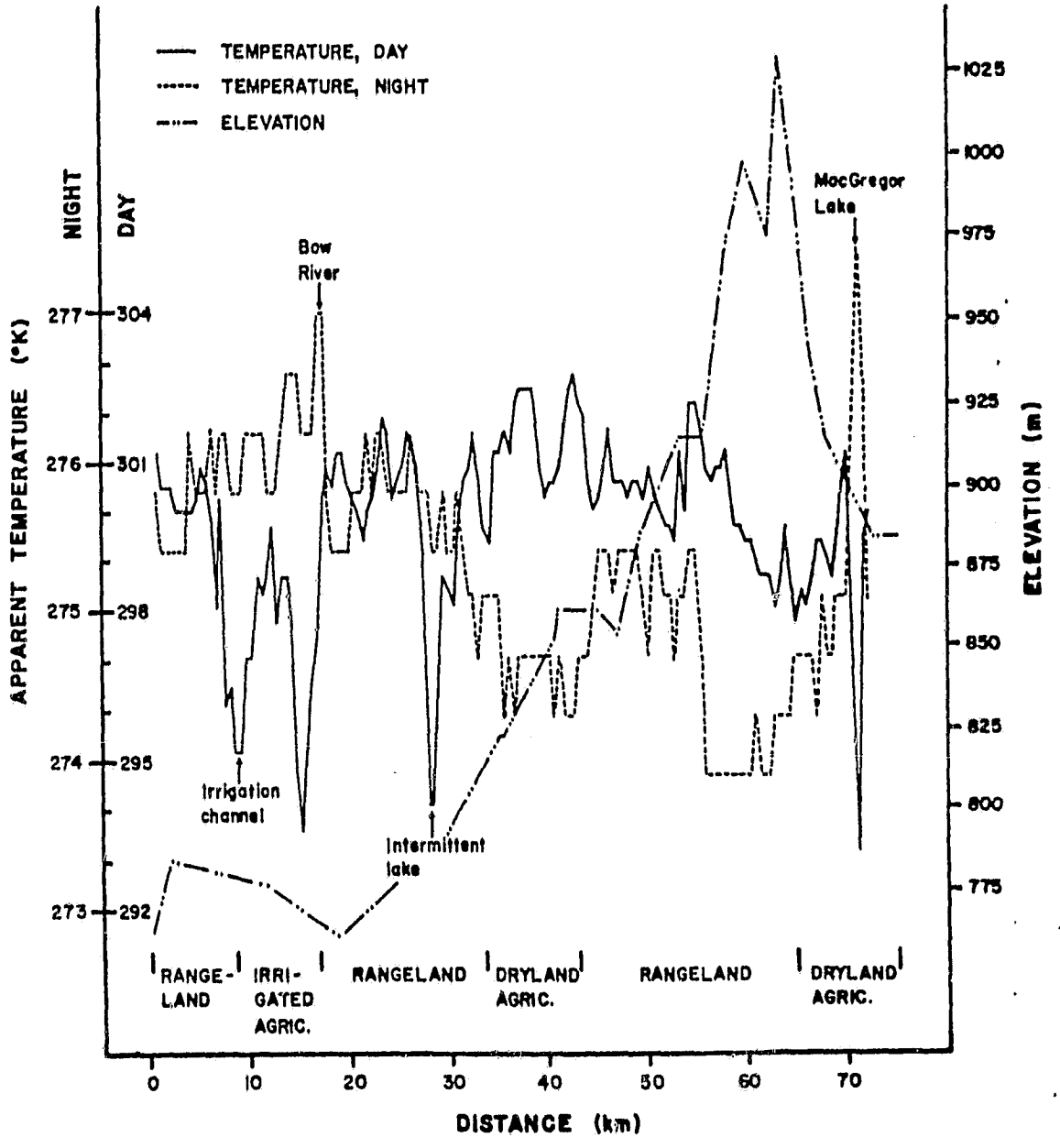

Figure 10: Profiles of elevation, surface cover, nighttime apparent temperature, and daytime apparent temperature for an area in southern Alberta. HCMM images were obtained 14 June, 1978.

TABLE 5

Correlation Coefficients Between API Results for Different k Values and 42 Southern Alberta Meteorological Stations - 14 June 1978

Values of k	0.75	0.80	0.85	0.90	0.90
0.75	1.00	0.99	0.97	0.94	0.88
0.80		1.00	0.99	0.97	0.93
0.85			1.00	0.99	0.96
0.90				1.00	0.99
0.95					1.00

(iii) meteorological stations from (ii) located in uniform areas; to qualify, the range of apparent thermal inertia values within a 3 x 3 matrix centred on the station had to be less than 11 for either resampling algorithm (6/6, 15/7); and

(iv) meteorological stations from (ii) for which Landsat data were available (14/6).

Prior to calculations, HCMM digital data were converted into albedo (DVIS), day and night apparent temperature (DIR, NIR), and temperature difference (Δ T) using formulas given in Anonymous (1978). Full frame atmospheric corrections were not performed because no date-to-date comparisons were made and spatial data on atmospheric conditions were not available.

Correlation coefficients between API and satellite measurements calculated for three subsets of the 14 June, 1978 data are shown in Figure 11. Correlation coefficients were low for all HCMM data. In addition, r values should be negative for daytime temperature measurements but the opposite is true in Figure 11 for the nearest neighbour resampling algorithm. It is interesting to note that the cubic convolution resampling algorithm (pixel size 350 m) resulted in r values with the "expected" signs for subsets (ii) and (iv) while the nearest neighbour algorithm (pixel size 481.5 m) data provided opposite signs for the same group of meteorological stations. However, since with one exception (DVIS, NN resampling, N = 23), none of the HCMM r values shown in Figure 12 were significant at the 1% probability level, the significance of these differences is not clearly evident.

Figure 12 shows correlation coefficients calculated between API (k = 0.85) and HCMM data from 15 July, 1978 converted to albedo and apparent temperatures. Subsets of data representing meteorological station locations were selected using the criteria for subsets (i), (ii) and (iii) listed above. No suitable Landsat data were available for the July period. The results (Figure 12) show an expected behaviour of daytime temperature, temperature difference and thermal inertia for stations located in areas with uniform surface cover (subset (iii)). Daytime temperatures were consistently lower for higher API values but the r value for nighttime temperatures varied depending on the subset chosen. This is probably due to the range of temperatures encountered in the 15 July data (about 10°C for nighttime and 35°C for daytime values) which affected the stability of the relationship. The 15 July correlation coefficients behaved more consistently than the 14 June data, and both DIR and NIR r values (N =41) were statistically significant at the 5% probability level. They also showed little difference between the two resampling algorithms.

Correlation coefficients between API and HCMM measurements for the eastern site on 6 June, 1978 are shown in Figure 13. Only NN resampling was done on this site. The values are again fairly low and are not statistically significant.

AREA: SOUTHERN ALBERTA
DATE: JUNE 14, 1978
RESOLUTION: HCMM-NN: 481.5 M
HCMM-CC: 350.0 M
LANDSAT: 175.0 M
———●— N = 37
———○— N = 20
———▲— N = 23

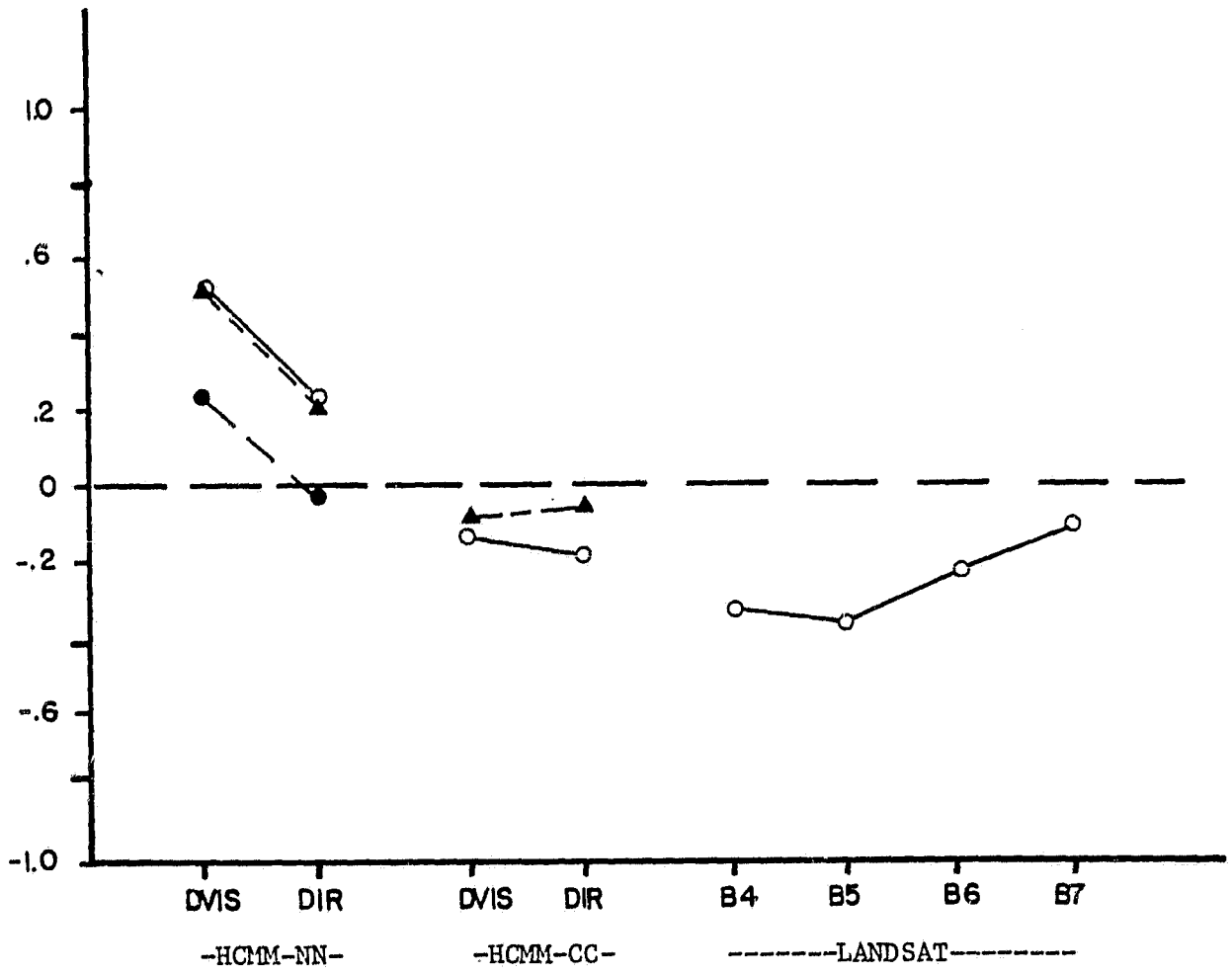

Figure 11: Correlation coefficients between API and satellite (HCMM, LANDSAT) measurements. 14 June, 1978, southern Alberta.

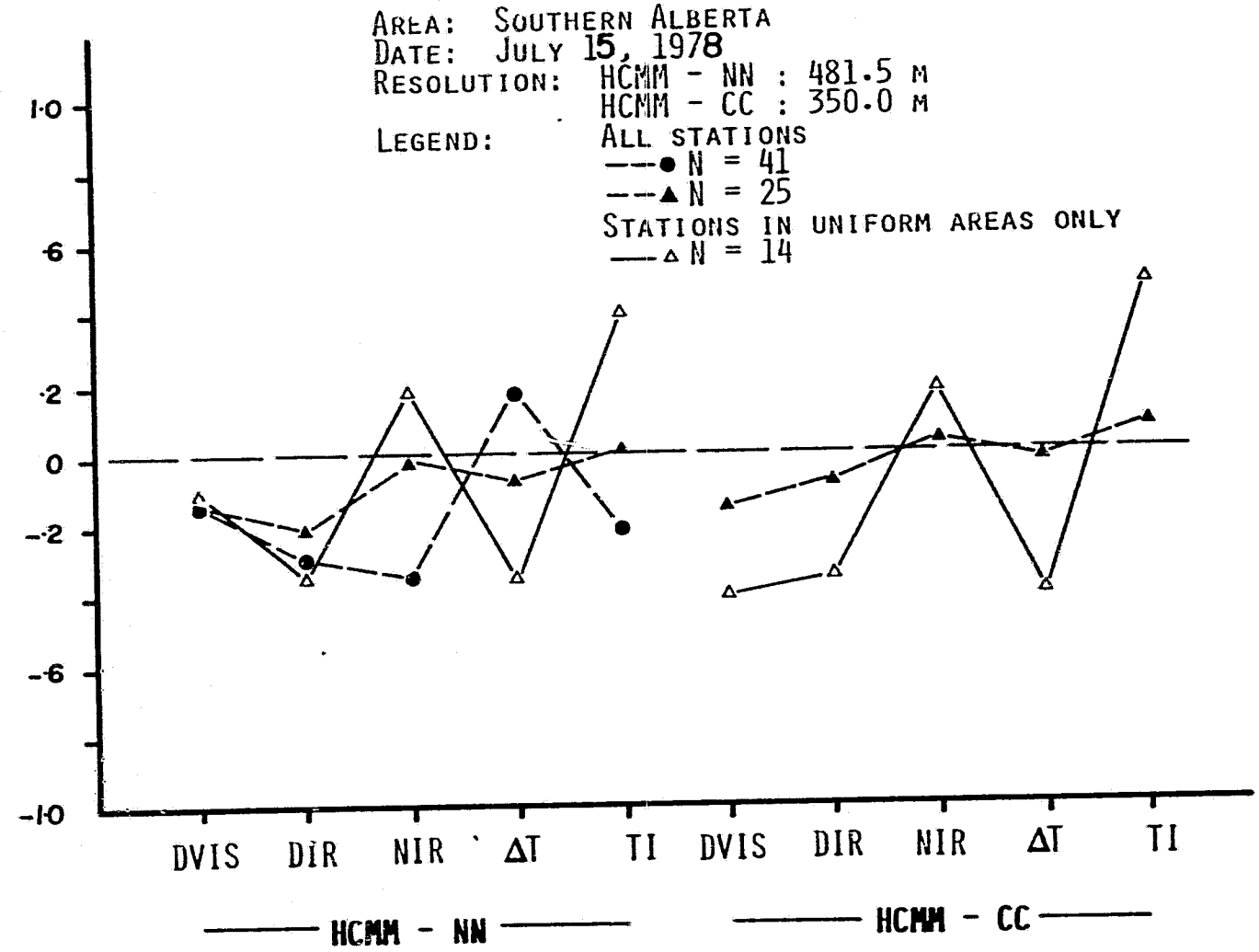

Figure 12: Correlation coefficients between API and HCMM measurements. 15 July, 1978, southern Alberta.

AREA: EASTERN CANADA
DATE: JUNE 6, 1978
RESOLUTION: HCMM-NN: 481.5 M
LEGEND: ALL STATIONS
———■ N = 63
STATIONS IN UNIFORM AREAS ONLY
——□ N = 32

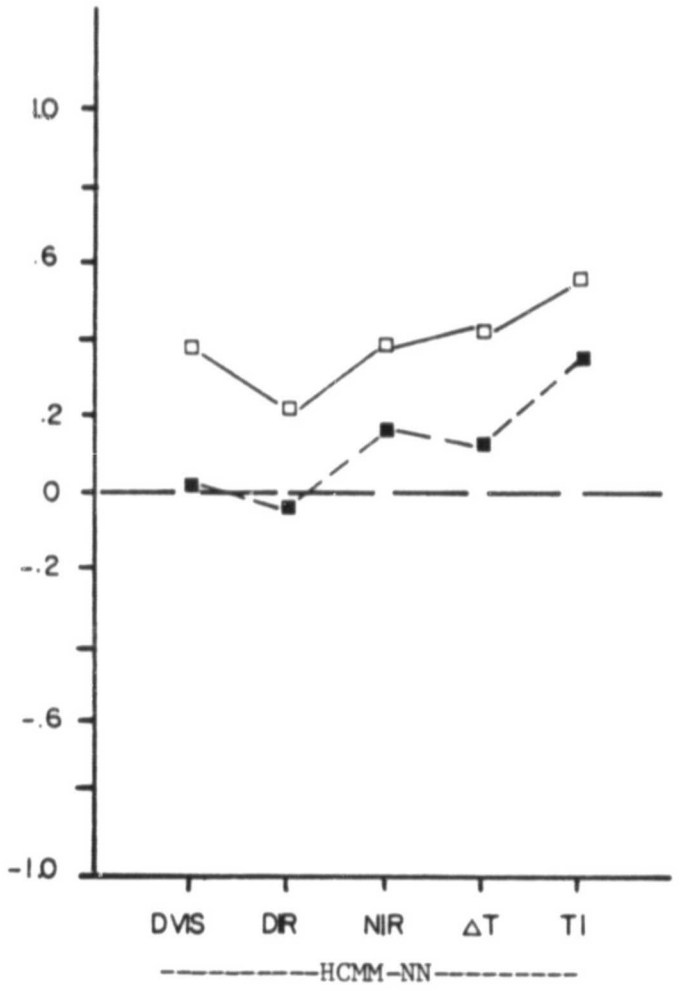

Figure 13: Correlation coefficients between API and HCMM measurements. 6 June 1978, eastern Canada.

Upon comparing results from Figure 11 to 13, several observations can be made. First, the albedo-API correlation was higher than the daytime temperature-API correlation for all subsets of both June dates. However, one would expect a negative correlation coefficient (higher API corresponding to lower albedo) instead of a positive one actually found. In July, the r value for albedo was close to zero. In addition, the June r values increased when more uniform subsets ((ii) and (iii)) were selected but in the "undesirable" direction. In July, the API correlation with daytime apparent temperature was better than with albedo, and also had the expected sign. Although most of the r values were not statistically significant, the consistence of the June-July trend suggest that it may be real and may represent the influence of heterogeneous surface cover in the HCMM data. Given the three dates of observation, there is only 16% probability that the decreasing r trend occurred by chance alone. Furthermore, the data represents two geographic sites which likely introduced further uncertainties. In July, agricultural areas are more uniform than in June and the effect of soil water on thermal IR emission could therefore be more clearly shown.

3.3 Cloud Cover Analysis

To evaluate the reliability of HCMM-type data for operational soil moisture and plant stress monitoring, the incidence of cloud cover was analyzed for both eastern and western sites. The analysis was carried out for June, July and August 1978, separately for day and night images. After a given thermal IR image was visually registered to a base map, cloud cover was estimated (10% increments) for geographical grid cells 1^{o} latitude $\times$ 1^{o} longitude in size. The average cloud cover per cell was then calculated and 20% contours were plotted. Where less than five images were available, the contours are shown as broken lines.

An analysis of the western site data (Figure 14a through 14f) showed the average cloud cover to be quite variable, both spatially and temporally. The variability is evident in Figure 8a through 8g which are relatively cloud-free images. Since the cloud cover is not only 0 or 100% but is more or less randomly distributed, this spatial variability renders many images unsuitable for a quantitative analysis of surface phenomena. In the daytime, cloud cover was heavy over Rocky Mountains in all three months; in southern Alberta and Saskatchewan, cloud cover varied between 40 and 60% (Figure 14a, c, e). The daytime values were generally lower in northern U.S. Nightime clouds were distributed differently; the values over the Rockies were generally below 40%, and higher values existed in southern Alberta and eastern Saskatchewan (Figure 14b, d, f).

Daytime cloud cover was higher in the eastern site, generally varying between 50 and 70% (Figure 15a, c, e). The values were lower in eastern Canada and northeastern U.S. Nighttime images (Figure 15b, d, f) showed lower values for the U.S. but over Canada clouds obscured the ground with a frequency of 50% or higher.

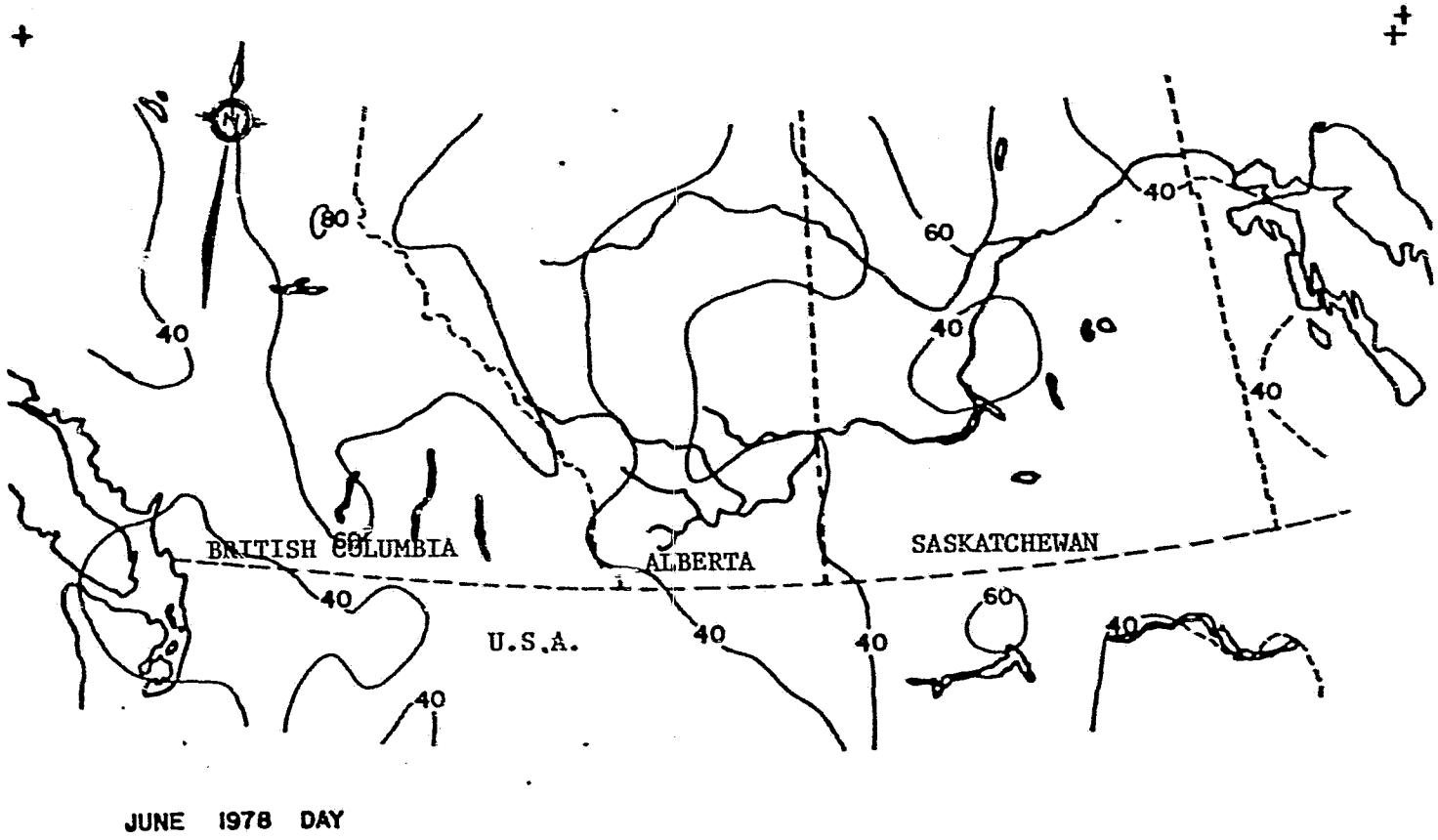

FIGURE 14a: Day cloud cover map (in percent) for the western site: June, 1978.

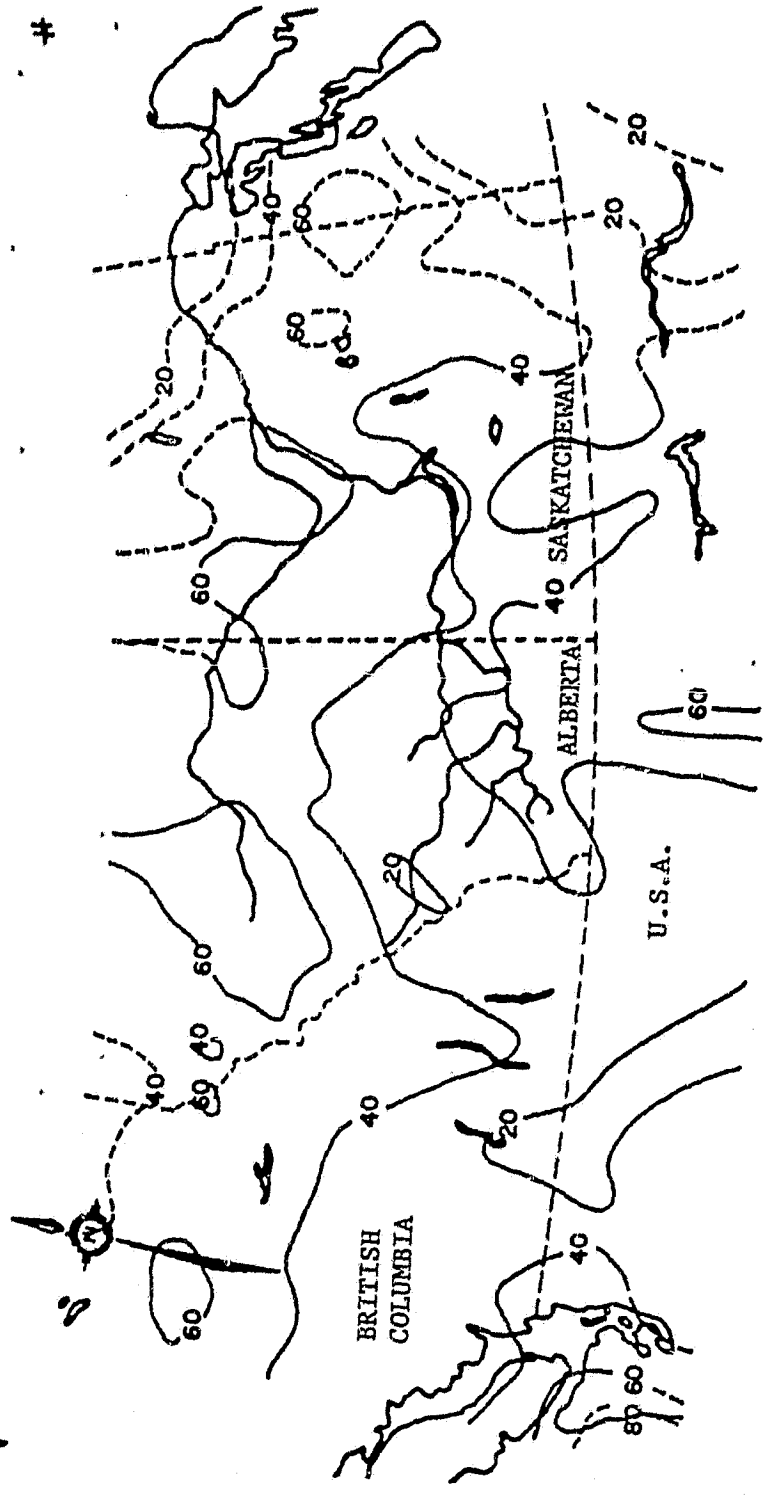

FIGURE 14b: Night cloud cover map (in percent) for the western site: June, 1978.

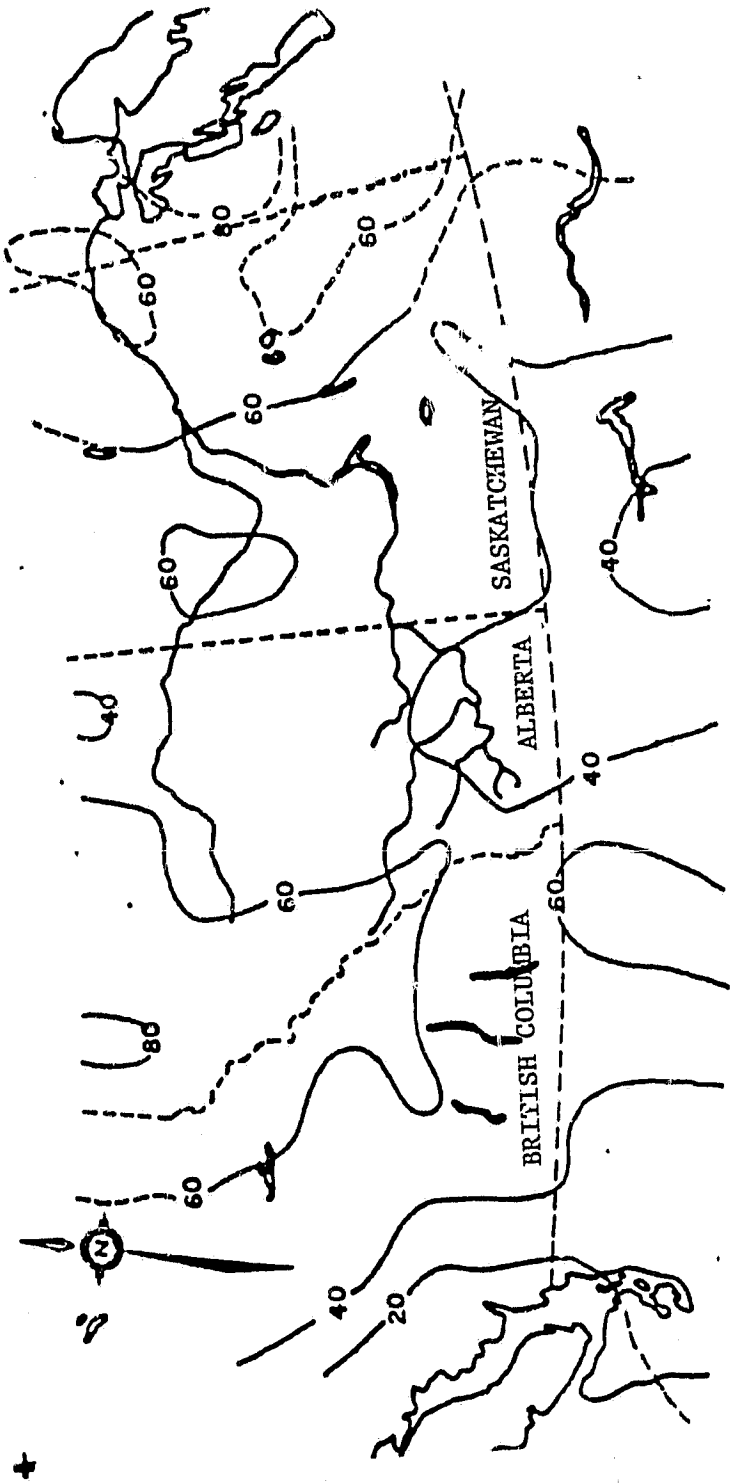

JULY 1978 DAY

FIGURE 14c: Day cloud cover map (in percent) for the western site: July, 1978.

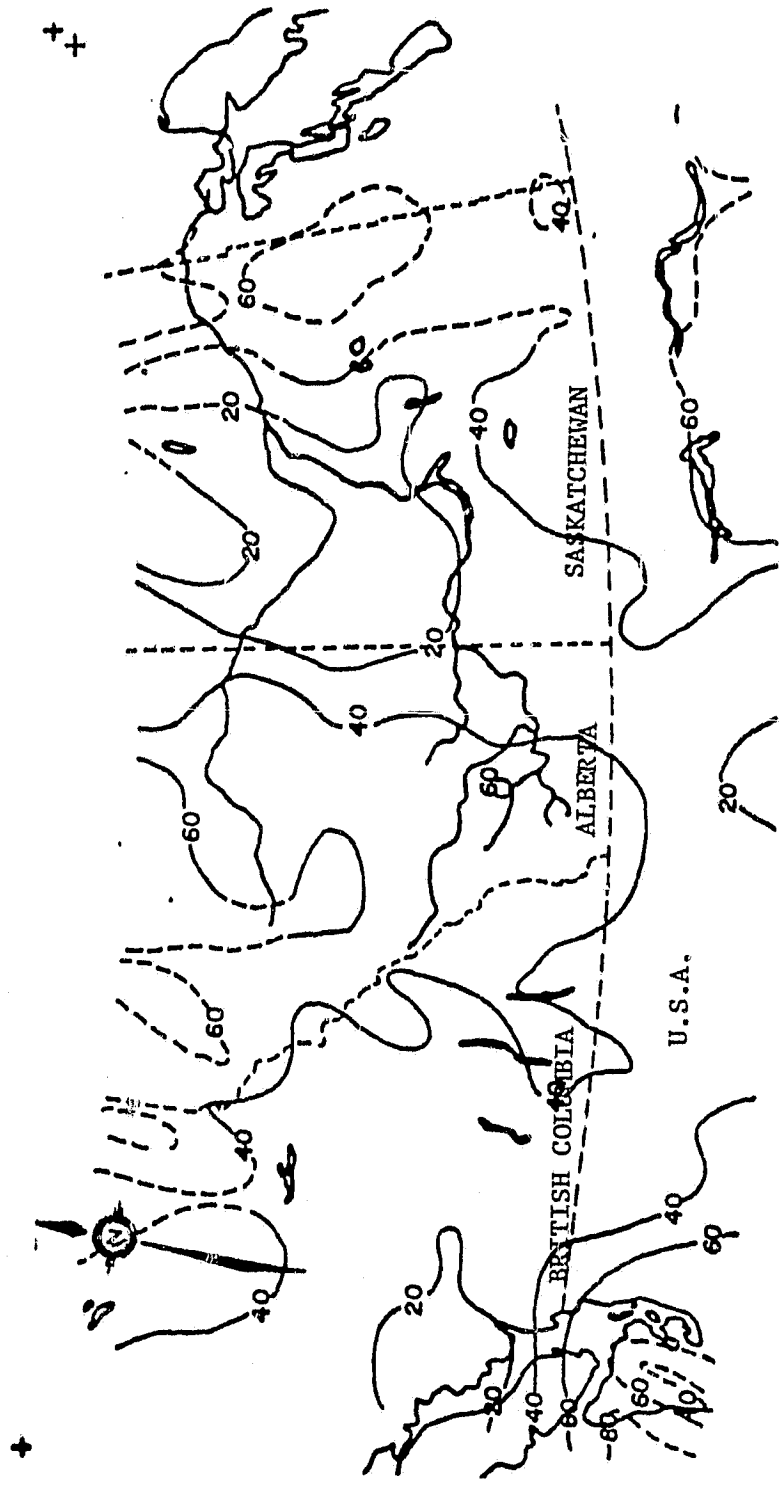

FIGURE 14d: Night cloud cover map (in percent) for the western site: July, 1978.

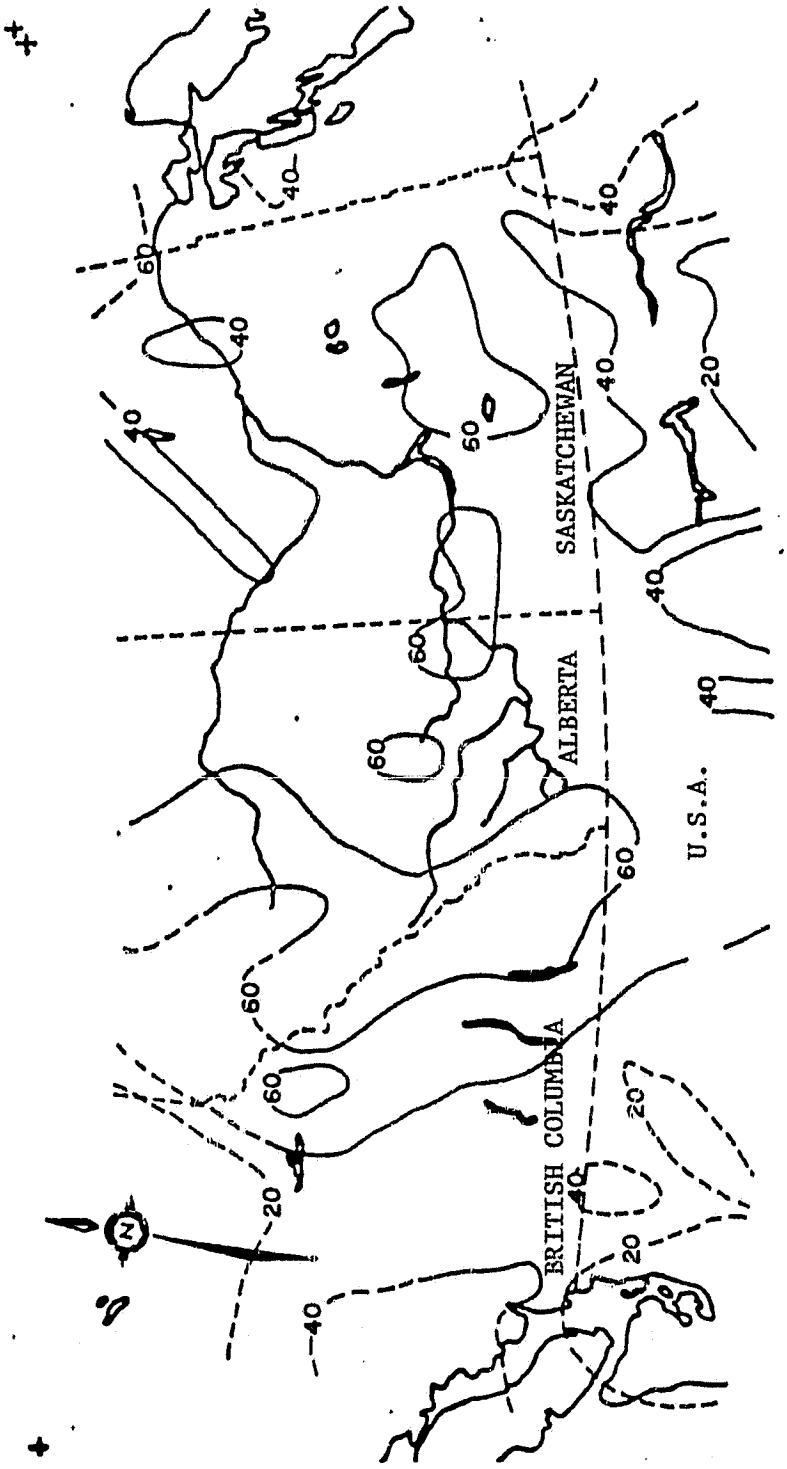

FIGURE 14e: Day cloud cover map (in percent) for the western site: August, 1978.

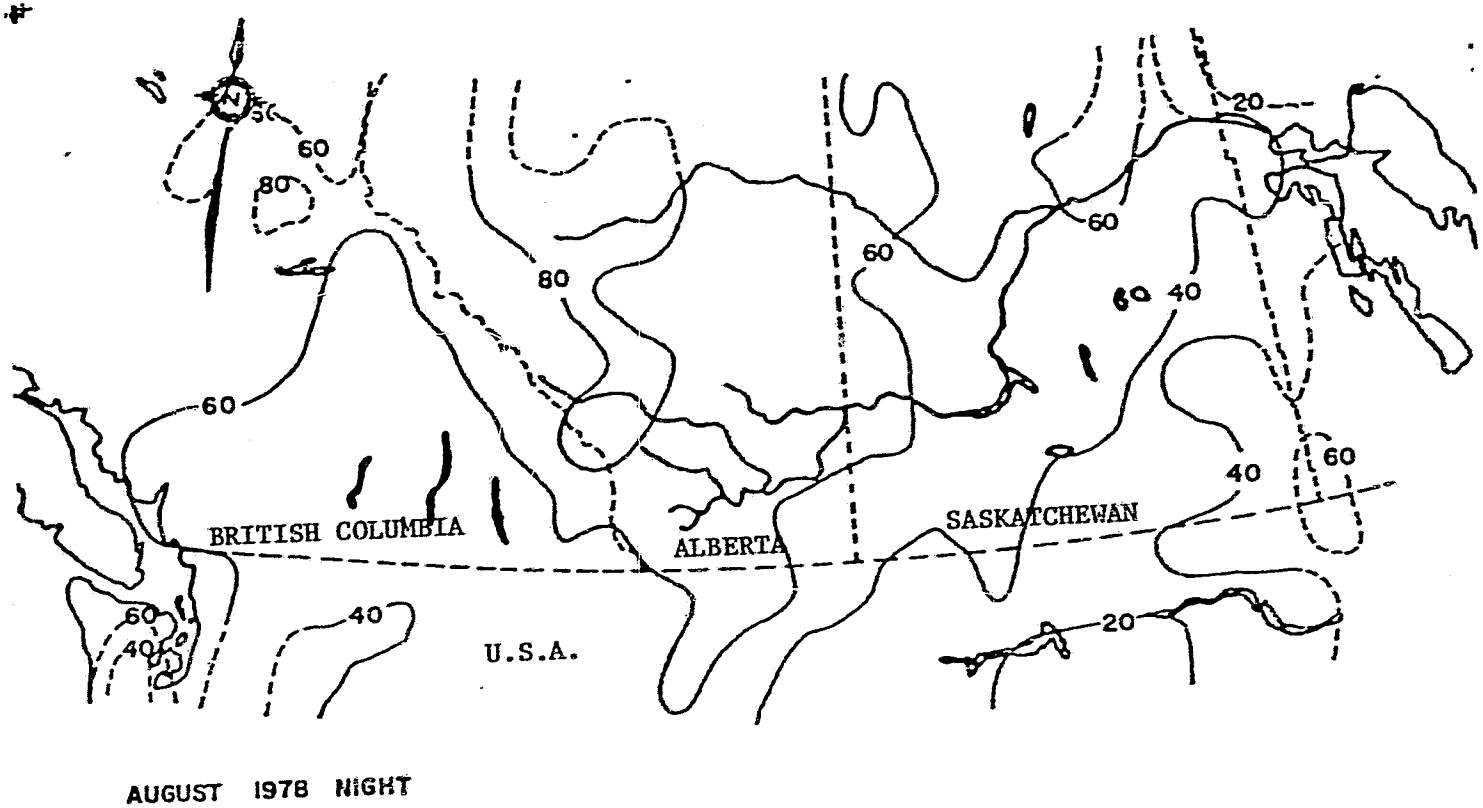

FIGURE 14f: Night cloud cover map (in percent) for the western site: August, 1978.

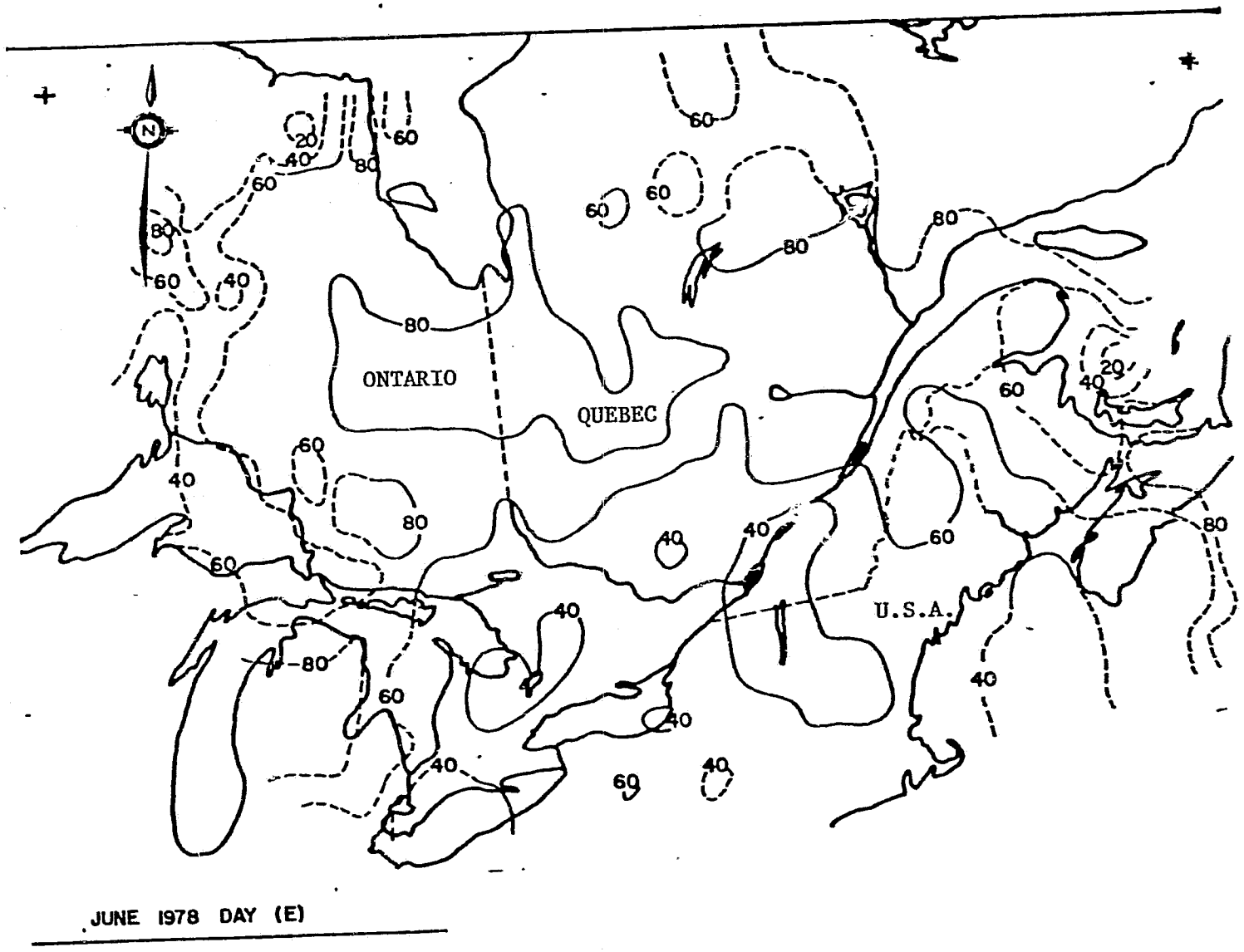

FIGURE 15a: Day cloud cover map (in percent) for the eastern site: June, 1978.

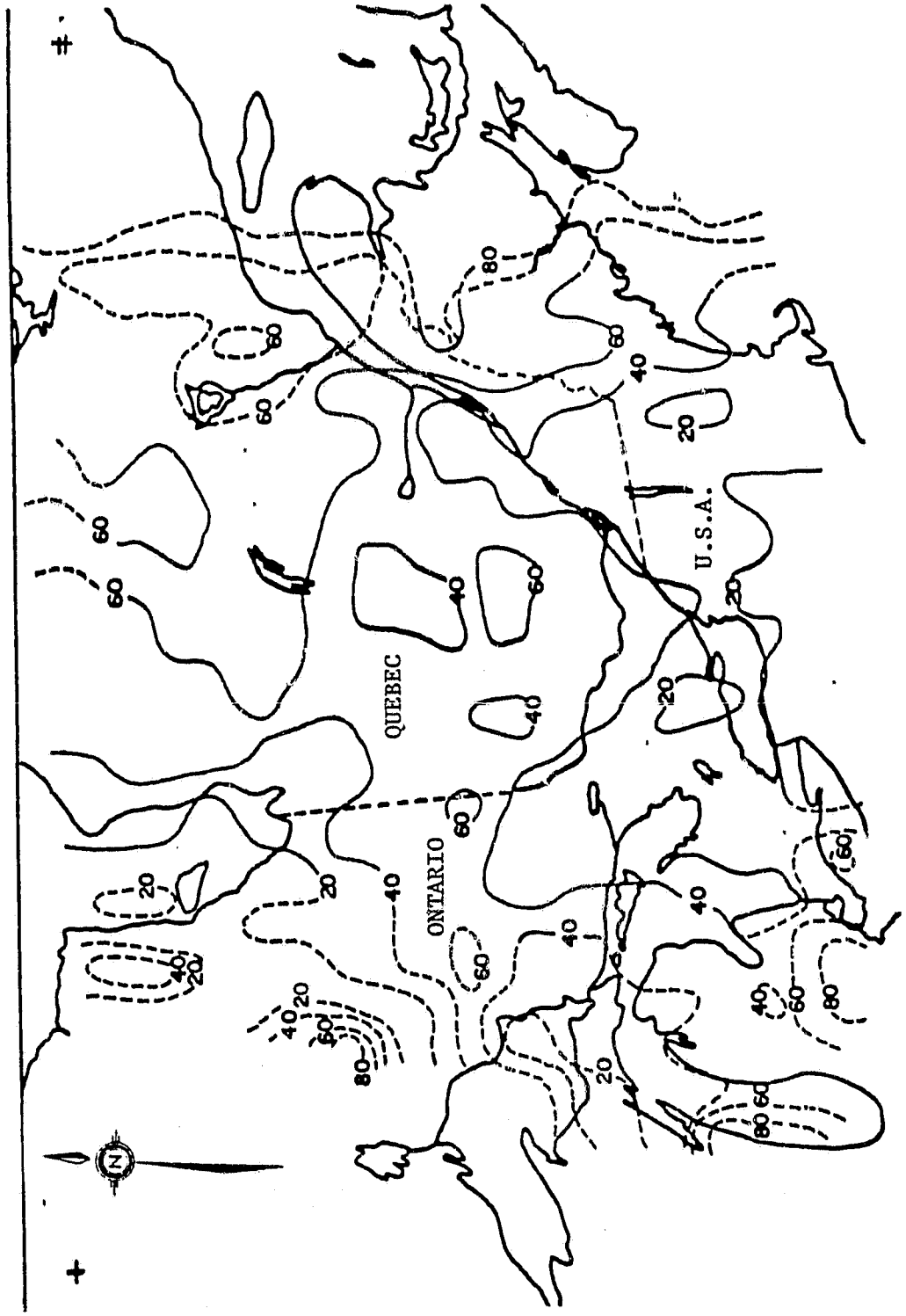

FIGURE 15b: Night cloud cover map (in percent) for the eastern site: June, 1978.

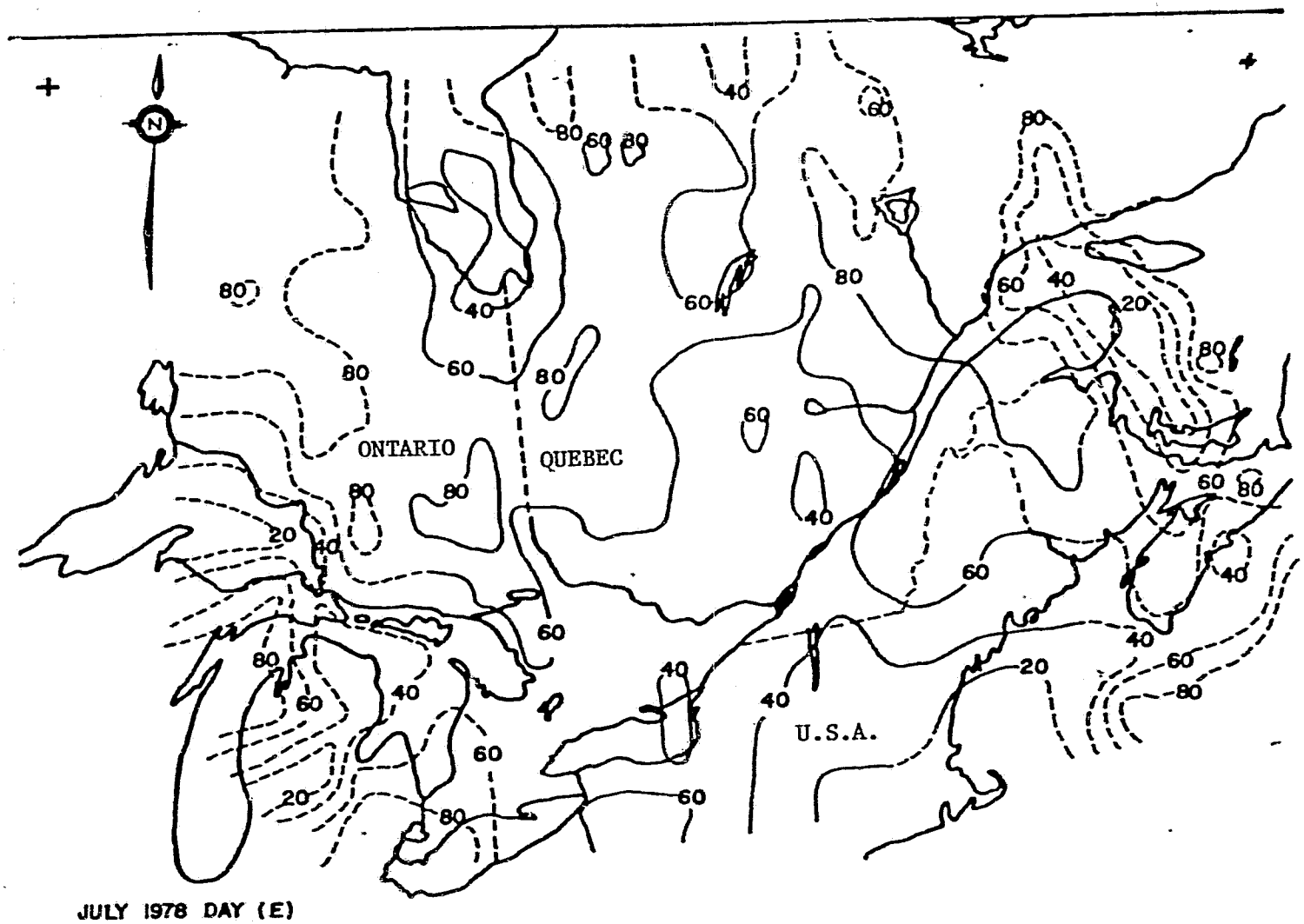

FIGURE 15c: Day cloud cover map (in percent) for the eastern site: July, 1978.

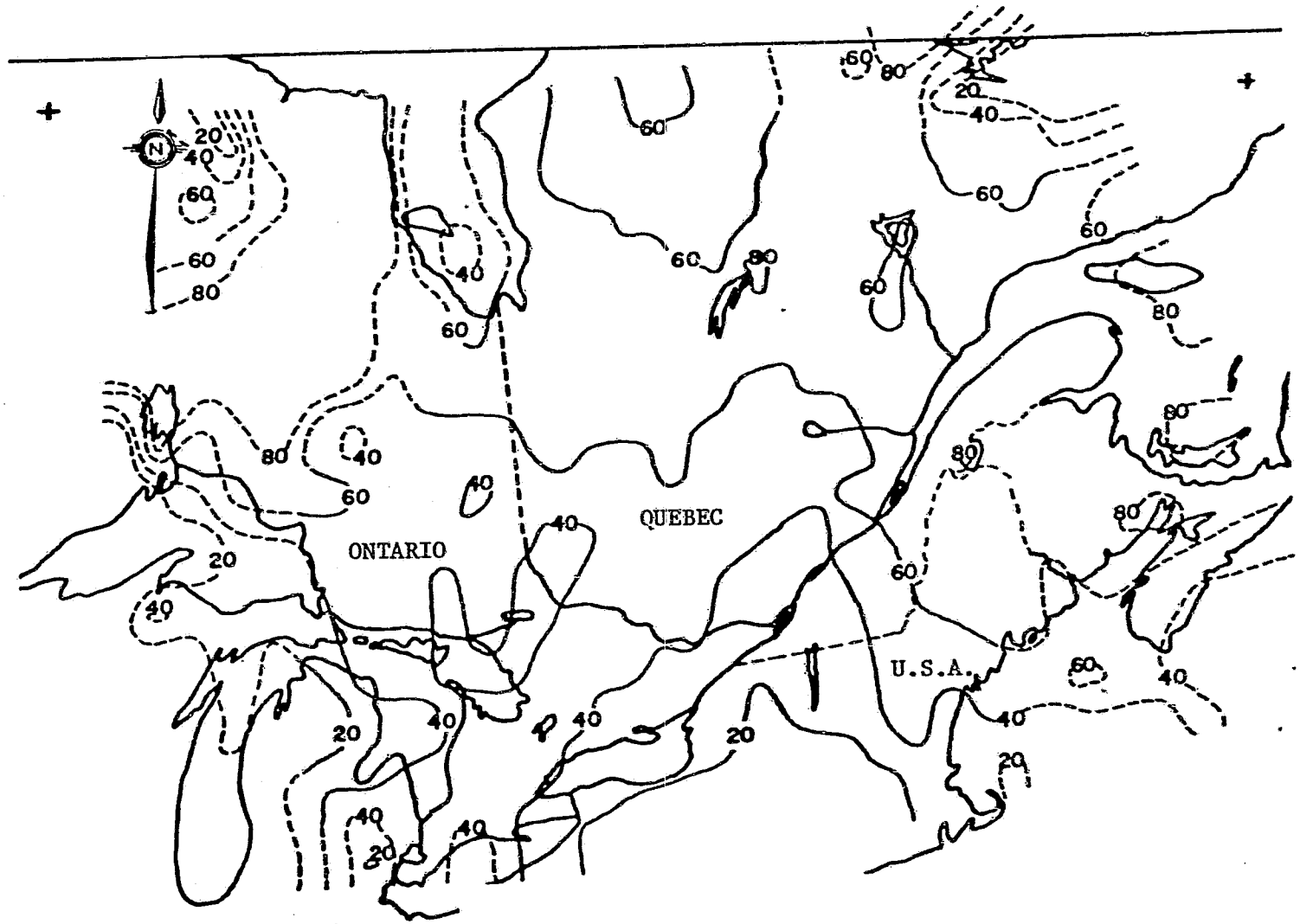

FIGURE 15d: Night cloud cover map (in percent) for the eastern site: July, 1978.

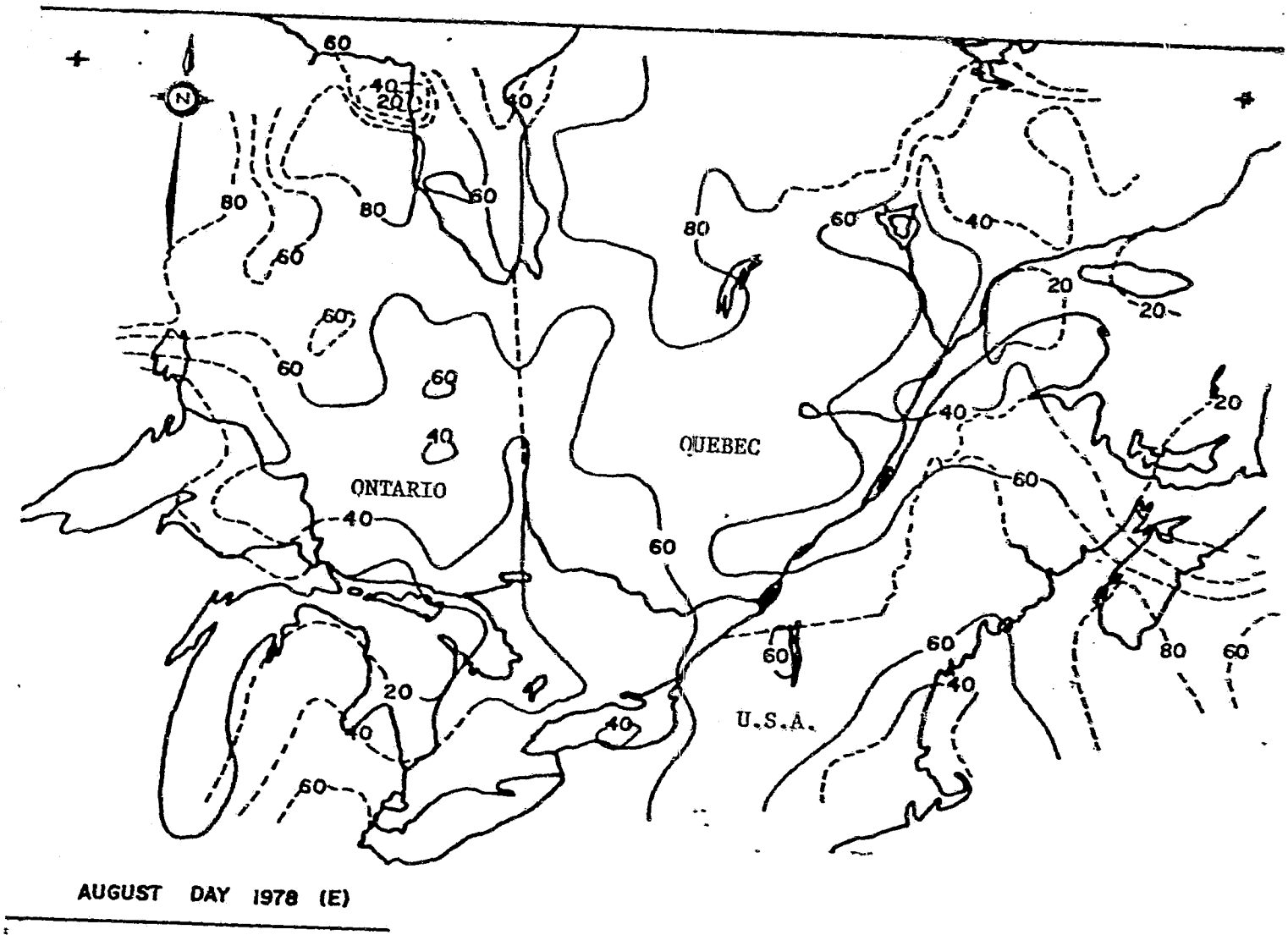

FIGURE 15e: Day cloud cover map (in percent) for the eastern site: August, 1978.

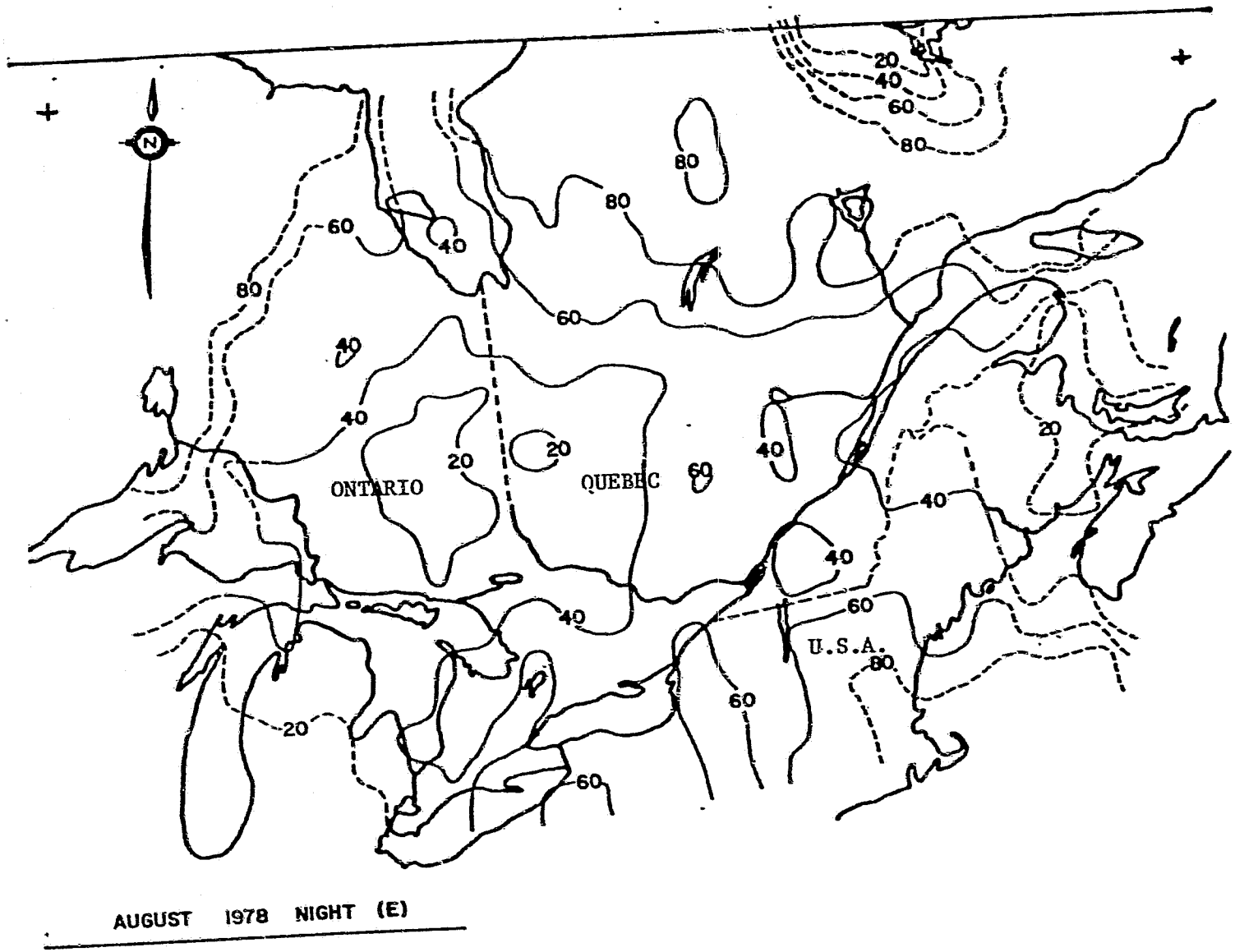

FIGURE 15f: Night cloud cover map (in percent) for the eastern site: August, 1978.

Since the day and night cloud distributions were different in the western site, the availability of day/night coverage would be considerably reduced compared to either coverage separately. Since an accurate delineation of subvisible clouds was not possible, the actual cloud cover (contaminated data) was probably underestimated. In general, very few images contained large cloud-free areas. On the other hand, many daytime images included some cloud-free areas in which the data were apparently not contaminated. To use these data effectively in a routine manner, two steps would be required. First, contaminated data would have to be corrected or deleted (preferably automatically). Information contained in the scene as well as ancilliary data (such as expected values of surface temperatures based on the season, time of day, etc.) could be used in this process. Second, the uncontaminated data would have to be geocoded. The latter operation is necessary because the cloud-free areas are often too small to be accurately located relative to land surface features.

3.4 Supporting Evidence

Four diurnal sets of airborne data were collected in a related experiment (Table 2). Following procedures described in Section 2, airborne and associated ground measurements were assembled and subjected to a regression analysis. Of particular interest was the relationship between Plant Available Water (PAW) and ΔT_{da} defined as the difference between the maximum apparent surface temperature and the maximum air temperature for the same diurnal period. In addition, the effect of plant cover was also examined as it was previously shown to be significant (Cihlar, 1980c).

To evaluate the effect of soil water content, July (1979) and August (1978 and 1979) data for one crop were merged whenever possible; plot and field data were also combined in this process. Due to the strong effect of partial plant cover in June, none of the June data were included in the regressions. The result was 11 data sets for the following crops: wheat (hard and soft), barley, dry beans, faba beans, alfalfa (seed), alfalfa (hay), cabbage, mustard, corn, canola (rapeseed), and potatoes. As an example, Figure 16 shows results for mustard. The inverse linear relationship between ΔT_{da} and PAW in July and August is well illustrated here.

After comparing regression results, it was noted that both intercepts and slopes of the regression lines differed among crops. The data were then grouped into five categories with similar regression parameters: (i) wheat, barley; (ii) dry beans, alfalfa seed; (iii) cabbage, mustard, faba beans; (iv) corn, alfalfa hay, canola; and (v) potatoes. Average regression parameters were calculated for each group to prepare Figure 17. With one exception, the regression lines exhibited similar slopes but different intercepts. The steep line represents dry beans and alfalfa seed and the reason for its different slope is not evident. It is also not clear why corn and alfalfa hay showed virtually no response to reduced soil water availability. One reason may be high relative humidity (low vapour pressure deficit) of the air above canopies of these irrigated crops. This paramater appears to have a strong effect on the magnitude of ΔT_{da} as it limits the maximum possible canopy - air temperature difference achievable under given crop stress conditions.

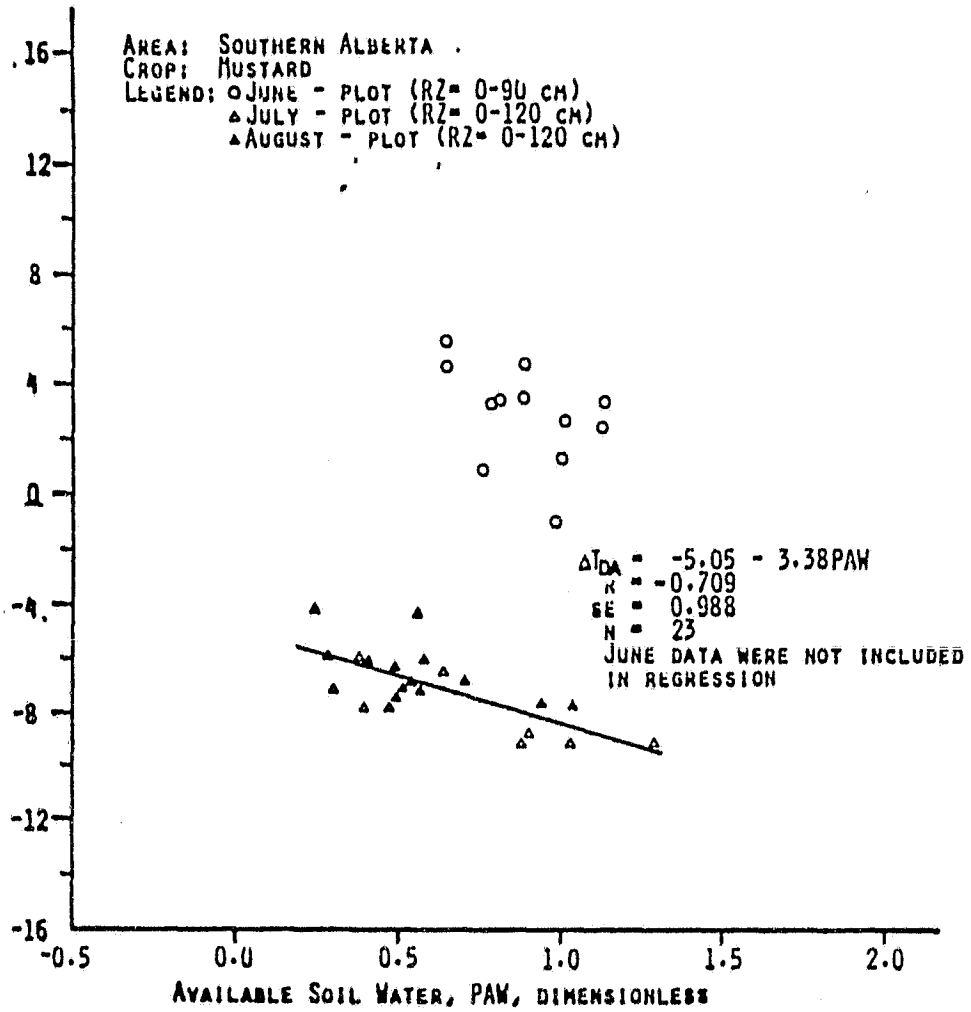

Figure 16: The relationship between available soil water and the daytime temperature difference T_{da} for mustard. Thermal IR data were acquired with an airborne scanner in southern Alberta.

AREA: SOUTHERN ALBERTA
LEGEND: ——— DRY BEANS
..... POTATOES
——— CABBAGE, MUSTARD, FABA BEANS
——— WHEAT, BARLEY
——— CORN, ALFALFA HAY, CANOLA

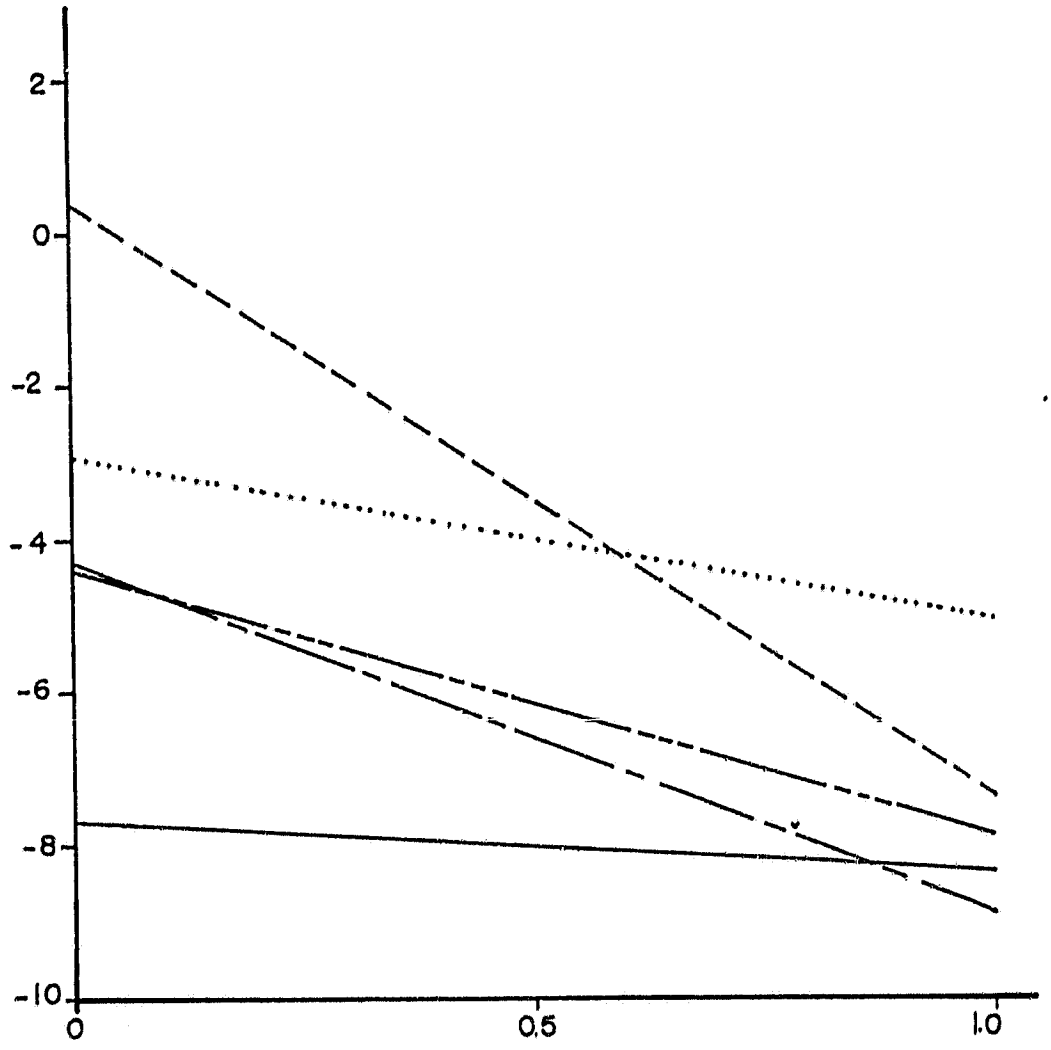

Figure 17: Regression lines representing the T_{da} vs. PAW relationship for five crop groups.

Using the regression parameters for the five crop groups, average values of slope, intercept, and standard error of the PAW vs. ΔT_{da} relationship were calculated. The average slope was -3.7°K/1.0 PAW, and the average standard error was 2.1°K. This means that for a given ΔT_{da} value, PAW could differ by up to 0.56 from its predicted value 66% of the time. In other words, the airborne data suggest that the ΔT_{da} vs. PAW relationship is not very closely defined.

To assess the effect of plant cover on ΔT_{da}, optical densities of the CIR transparencies were measured with Macbeth spot densitometer over the sampled sites. A parameter 10^{R-IR} was then calculated, where R and IR are densities of the red- and infrared-sensitive emulsion layers (measured with green and red filters), respectively. It can be shown that under certain simplifying assumptions 10^{R-IR} is proportional to an infrared to red reflectance ratio which has previously been determined to be closely correlated with green plant biomass (e.g., Tucker, 1977). To avoid interference caused by film processing and colour balance resulting from varying flight altitude, data were grouped according to film and flying height but all crops were combined for these calculations.

Figure 18 shows correlation coefficients between the daytime temperature diffference ΔT_{da} and the parameter 10^{R-IR}. Data for all crops at a given date were combined to calculate the correlation coefficients. It is evident that the correlation decreased between June and August for both plots and fields, but the r values were always lower for plots. It should be noted that the plots had more uniform cover than field sites and that the uniformity increased during the season for both sites. Because of this and since the infrared/red reflectance ratio tends to saturate at high biomass levels, correlation coefficients could be expected to decrease with time. However, for a partial ground cover in June, the plot correlation coefficients were higher than those between PAW and ΔT_{da}. The August 1978 data included dryland and irrigated fields with a wide range of ground cover, and the correlation also remained quite high.

4. SUMMARY AND CONCLUSIONS

Results of this study provided some evidence about the possibility of monitoring soil water status by means of satellite thermal IR sensing but also pointed out several significant problems. The temporal trend of correlations between API and daytime apparent temperature (Section 3.2.2) suggests that the soil water status may have a detectable effect on the daytime apparent temperatures. It is likely that these relationships were not sufficiently strong in part because of the large pixels containing a mix of surface cover types. This suggestion is supported by the existence of such a relationship for individual crops established using airborne thermal IR data.

Increasing spatial resolution of the satellite thermal IR data would overcome the problem of mixed cover types and several others. In particular, the coarse resolution makes it very difficult to select an appropriate parameter describing the soil water status

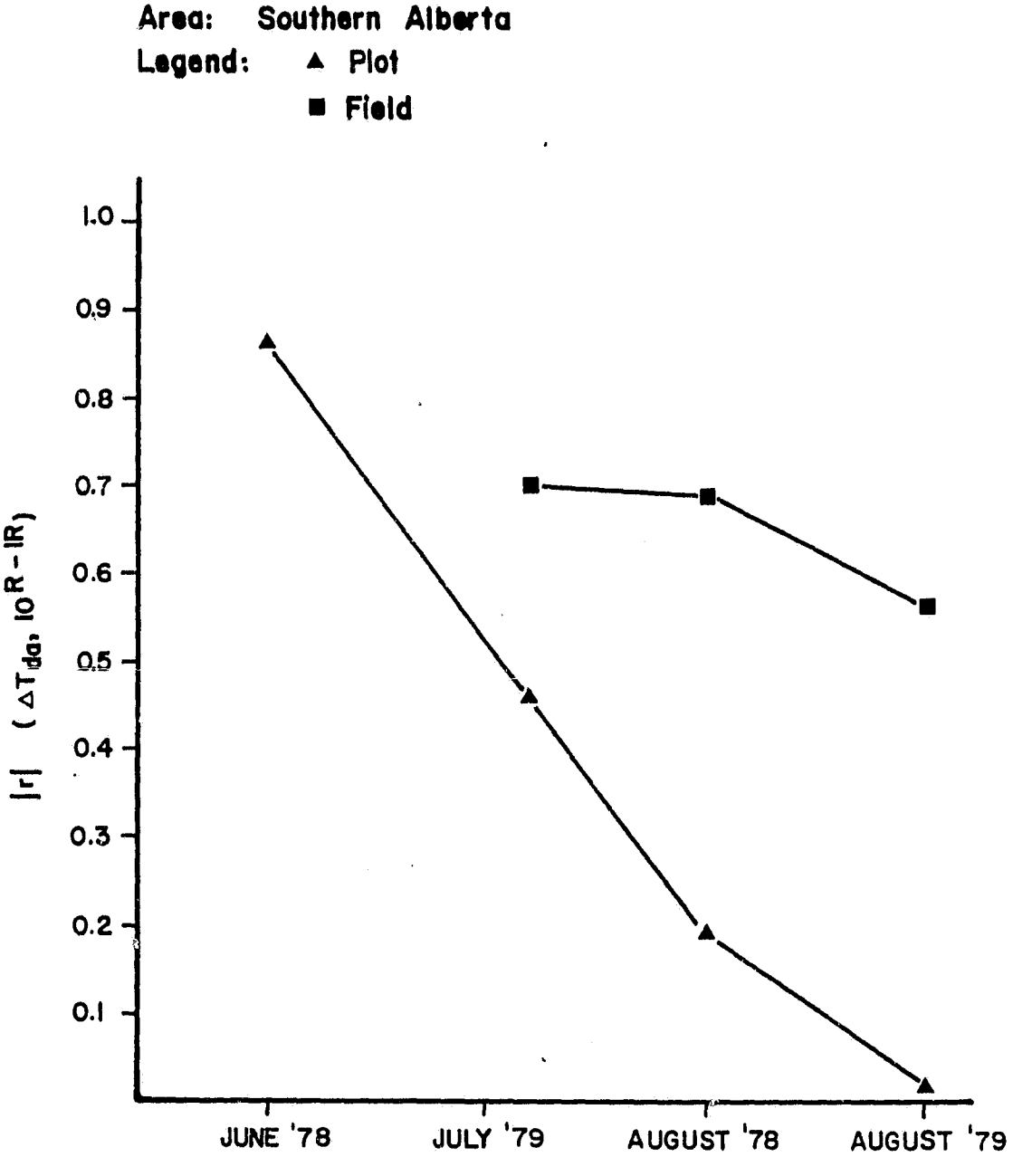

FIGURE 18: Correlation coefficient between T_{da} and 10^{R-IR} as a function of time.

because of the different depth sensitivities of the apparent temperature measurements for bare and vegetated surfaces. Secondly, the relative soil and vegetation contributions of bare, partly covered, and fully vegetated surfaces existing within a single pixel cannot be separated using HCMM-like data. However, resolving the partial cover ambiguity may be possible, at least in a relative sense (Klaasen and Nieuwenhuis, 1978). A further problem indicated by the airborne data is the relatively small ΔT_{da} sensitivity to soil water status as described by PAW (Section 3.4). A soil moisture estimating algorithm would also have to consider the relatively strong effects of surface cover and large altitudinal differences (Section 3.2.1) on the daytime apparent temperature.

Assuming that appropriate satellite data are available to develop a practically useful algorithm for describing soil water status, the problem of cloud contamination of the thermal data will have to be resolved. An automatic removal of irretrievably degraded pixels and geocoding of the uncontaminated data would yield a subset suitable for analysis. However, given the high cloud cover encountered in large areas of southern Canada and northern U.S. (Section 3.3), thermal IR satellite data could form only a supplementary data source in an operational soil moisture monitoring system.

A qualitative temporal analysis of many HCMM images established the importance of atmospheric, meteorological, topographic, and surface cover variables on the recorded thermal radiation. These results suggest that HCMM-type data should be of major value to regional climatological and meteorological studies and should also assist in identifying and describing the properties of surface cover types and materials. While in the latter case they would supplement data obtained in the visible and near-infrared part of the spectrum, they can be considered a unique data source for the regional climatological applications.

5. REFERENCES

1. Anonymous, 1980. Heat Capacity Mapping Mission (HCMM) Data Users Handbook. Prepared by the Goddard Space Flight Center, National Aeronautics and Space Administration, Greenbelt, Maryland. 120p.

2. Cihlar, J., 1978. Soil Moisture Information Needs and Remote Sensing Capabilities. Remote Sensing News Briefs, Energy, Mines and Resources Canada. 6p.

3. Cihlar, J., 1979. Remote sensing of soil moisture: techniques and applications in: "Applications of Remote Sensing in the Physical Environment", Climatological Research Series No. 12, McGill University, Montreal: 31-38.

4. Cihlar, J., 1979. HCMM/Soil Moisture Experiment. Progress Report, 31 August, 1979, Canada Centre for Remote Sensing. 10p.

ORIGINAL PAGE IS
OF POOR QUALITY

5. Cihlar, J., T. Sommerfeldt, and B. Paterson, 1979. Soil Water Content Estimation in Fallow Fields From Airborne Thermal Scanner Measurements. Canadian Journal of Remote Sensing 5: 18-32.

6. Cihlar, J. 1980a. HCMM/Soil Moisture Experiment. Progress Report, 30 April, 1980, Canada Centre for Remote Sensing. 4p.

7. Cihlar, J. 1980b. HCMM/Soil Moisture Experiment. Progress Report, 31 August, 1980, Canada Centre for Remote Sensing. 3p.

8. Cihlar, J. 1980c. Soil Water and Plant Canopy Effects on. International Journal of Remote Sensing (1) 2: 167-173.

9. Goodenough, D.G., 1979. The Image Analysis System (CIAS) at the Canada Centre for Remote Sensing. Canadian Journal of Remote Sensing 5: 3-17.

10. Jackson, R.D., J. Cihlar, J.E. Estes, J.L. Heilman, A. Kahle, E.T. Kanemasen, J. Millard, J.C. Price, and C.L. Wiegand, 1978. Soil Moisture Estimating Using Reflected Solar and Emitted Thermal Infrared Radiation. Chapter 4 in Heilman, J.L. et al (Eds.), Soil Moisture Workshop, NASA Conference Publication 2073: 4-1 to 4-47.

11. Klaasen, W., and G.J.A. Nieuwenhuis, 1978. Estimation of the regional evapotranspiration from remotely sensed crop surface temperatures. Part II: Arable Land. Note 1057, Instituut roor Cultuurtechniek en Waterhuishouding, Wageningen. 29p.

12. McFarland M.J., 1976. The Correlation of Skylab L-Band Brightness Temperatures with Antecedent Precipitation. Proceedings of the Conference on Hydrometeorology, Fort Worth, Texas: 60-65.

13. McFarland, M.J., and B.J. Blanchard, 1977. Temporal Correlations of Antecedent Precipitation with Nimbus-5 ESMR Brightness Temperatures. Proceedings of the Second Conference on Hydrometeorology, Toronto, Ontario: 311-315.

14. Schmugge, T.J., J.M. Meneely, A. Rango, and R. Neff, 1977. Satellite Microwave Observations of Soil Moisture Variations. Water Resources Bulletin 13: 265-281.

15. Tucker, C.J., 1977. Use of Near-Infared/Red Radiance Ratios for Estimating Vegetation Biomass and Physiological Staatues. Report X-923-77-183, NASA Goddard Space Flight Center, Greenbelt, Maryland. 41p.